Life Sciences 314 (2023) 121325

Contents lists available at ScienceDirect

Life Sciences

journal homepage: www.elsevier.com/locate/lifescie

Combined metabolic activators improve metabolic functions in the animal models of neurodegenerative diseases

Hasan Turkez [a,1], Ozlem Altay [b,1], Serkan Yildirim [c], Xiangyu Li [b], Hong Yang [b], Cemil Bayram [d], Ismail Bolat [c], Sena Oner [e], Ozlem Ozdemir Tozlu [e], Mehmet Enes Arslan [e], Muhammad Arif [b], Burak Yulug [f], Lutfu Hanoglu [g], Seyda Cankaya [f], Simon Lam [h], Halil Aziz Velioglu [i,j], Ebru Coskun [g], Ezgi Idil [f], Rahim Nogaylar [f], Ahmet Ozsimsek [f], Ahmet Hacimuftuoglu [d], Saeed Shoaie [b,h], Cheng Zhang [b,k], Jens Nielsen [l], Jan Borén [m], Mathias Uhlén [b,*], Adil Mardinoglu [b,h,**]

[a] Department of Medical Biology, Faculty of Medicine, Atatürk University, Erzurum, Turkey
[b] Science for Life Laboratory, KTH Royal Institute of Technology, Stockholm, Sweden
[c] Department of Pathology, Veterinary Faculty, Ataturk University, Erzurum, Turkey
[d] Department of Medical Pharmacology, Faculty of Medicine, Atatürk University, Erzurum, Turkey
[e] Department of Molecular Biology and Genetics, Faculty of Science, Erzurum Technical University, Erzurum, Turkey
[f] Department of Neurology and Neuroscience, Faculty of Medicine, Alanya Alaaddin Keykubat University, Antalya, Turkey
[g] Department of Neurology, Faculty of Medicine, Istanbul Medipol University, Istanbul, Turkey
[h] Centre for Host-Microbiome Interactions, Faculty of Dentistry, Oral & Craniofacial Sciences, King's College London, London, United Kingdom
[i] Functional Imaging and Cognitive-Affective Neuroscience Lab, Istanbul Medipol University, Istanbul, Turkey
[j] Department of Women's and Children's Health, Karolinska Institute, Neuroimaging Lab, Stockholm, Sweden
[k] School of Pharmaceutical Sciences, Zhengzhou University, Zhengzhou, PR China
[l] Department of Biology and Biological Engineering, Chalmers University of Technology, Gothenburg, Sweden
[m] Department of Molecular and Clinical Medicine, University of Gothenburg and Sahlgrenska University Hospital, Gothenburg, Sweden

ARTICLE INFO

Keywords:
Neurodegenerative diseases
Combined metabolic activators
Genome-scale metabolic model
Animal model

ABSTRACT

Background: Neurodegenerative diseases (NDDs), including Alzheimer's disease (AD) and Parkinson's disease (PD), are associated with metabolic abnormalities. Integrative analysis of human clinical data and animal studies have contributed to a better understanding of the molecular and cellular pathways involved in the progression of NDDs. Previously, we have reported that the combined metabolic activators (CMA), which include the precursors of nicotinamide adenine dinucleotide and glutathione can be utilized to alleviate metabolic disorders by activating mitochondrial metabolism.

Methods: We first analysed the brain transcriptomics data from AD patients and controls using a brain-specific genome-scale metabolic model (GEM). Then, we investigated the effect of CMA administration in animal models of AD and PD. We evaluated pathological and immunohistochemical findings of brain and liver tissues. Moreover, PD rats were tested for locomotor activity and apomorphine-induced rotation.

Findings: Analysis of transcriptomics data with GEM revealed that mitochondrial dysfunction is involved in the underlying molecular pathways of AD. In animal models of AD and PD, we showed significant damage in the high-fat diet groups' brain and liver tissues compared to the chow diet. The histological analyses revealed that hyperemia, degeneration and necrosis in neurons were improved by CMA administration in both AD and PD animal models. These findings were supported by immunohistochemical evidence of decreased

* Corresponding author.
** Correspondence to: A. Mardinoglu, Centre for Host-Microbiome Interactions, Faculty of Dentistry, Oral & Craniofacial Sciences, King's College London, London, United Kingdom.
E-mail addresses: havva.altay@scilifelab.se (O. Altay), syildirim@atauni.edu.tr (S. Yildirim), xiangyu.li@scilifelab.se (X. Li), hong.yang@scilifelab.se (H. Yang), ismail.bolat@atauni.edu.tr (I. Bolat), ozlem.ozdemir@erzurum.edu.tr (O.O. Tozlu), muhammad.arif@scilifelab.se (M. Arif), lhanoglu@kure.com.tr (L. Hanoglu), simon.1.lam@kcl.ac.uk (S. Lam), ahmeth@atauni.edu.tr (A. Ozsimsek), saeed.shoaie@scilifelab.se (S. Shoaie), cheng.zhang@scilifelab.se (C. Zhang), nielsenj@chalmers.se (J. Nielsen), Jan.Boren@wlab.gu.se (J. Borén), mathias.uhlen@scilifelab.se (M. Uhlén), adilm@scilifelab.se (A. Mardinoglu).
[1] Contributed equally.

https://doi.org/10.1016/j.lfs.2022.121325
Received 28 September 2022; Received in revised form 13 December 2022; Accepted 21 December 2022
Available online 26 December 2022

immunoreactivity in neurons. In parallel to the improvement in the brain, we also observed dramatic metabolic improvement in the liver tissue. CMA administration also showed a beneficial effect on behavioural functions in PD rats.

Interpretation: Overall, we showed that CMA administration significantly improved behavioural scores in parallel with the neurohistological outcomes in the AD and PD animal models and is a promising treatment for improving the metabolic parameters and brain functions in NDDs.

1. Introduction

Neurodegenerative diseases (NDDs), including Alzheimer's disease (AD) and Parkinson's disease (PD), are progressive disorders that affect >50 million people globally [1]. Protein aggregation, oxidative stress, neuroinflammation, and blood-brain barrier dysfunction are typical molecular and cellular hallmarks of NDDs, leading to neuronal damage and cognitive decline [2]. In this context, mitochondrial dysfunction causes unfavourable neurophysiological events such as neuronal loss and synaptic impairment, which results in NDD [3,4]. Numerous studies over years have identified the connections between metabolic abnormalities and pathophysiological pathways in the brain [3,5–11]. For instance, previous multi-omics studies have shown reduced chaperone proteins [12] and dysregulated genes associated with mitochondrial energy metabolisms such as complex I–IV, ATP synthase, and cytochrome C oxidase [13,14]. A recent study evaluating the transcriptomic and proteomic levels of patients with PD suggested that disease should be considered a disturbance of complex biologic systems [15]. Moreover, several dynamic neuroimaging studies have indicated that PD is characterized by critical cognitive network alterations, particularly in salience network activity [16–18]. Despite these promising studies, no research has evaluated fundamental common pathophysiological mechanisms shared by systemic metabolic alterations and activities in specific brain areas in NDD pathogenesis [19]. Therefore, there is an unmet need for identification of the neurobiological processes underlying each condition.

Several lines of evidence suggest that neuroprotective strategies are becoming relevant to slow down inflammatory processes related to progressive neurodegeneration. For instance, it has been suggested that NAD+ precursors might be beneficial to improve age-related metabolic impairment and morbidities. As an example, a recent study showed that boosting NAD+ through the nicotinamide riboside (NR) enhances mitochondrial activity in patient neurons [10]. A recent phase I study of NAD supplementation with NR in PD showed an improved brain metabolism [3,11]. Moreover, growing data indicate significant mitochondrial dysfunction occurs early in AD pathogenesis. Therefore, mitochondrial impairment suggests a reasonable biological explanation for the brain hypofunction that accompanies AD-related pathologies and provides treatment options for AD and other NDDs.

Animal models of NDDs have significantly improved our understanding of the molecular pathogenesis of the diseases. Moreover, rigorous use of models that more accurately mimic human disease can enhance our translational knowledge about the disease and enforce the development of mechanistically tailored therapies. Recent studies have shown that high-fat diet (HFD) damages crucial brain regions involved in cognition, which are compromised in NDDs [20–23]. Among the various causes of HFD associated memory impairment, neuroinflammation appears to have a critical role in the occurrence of the disease. The elevated neuroinflammatory response in HFD mice is linked to increased blood-brain barrier (BBB) permeability [24]. Furthermore, HFD is also associated with motor deficits and behavioural changes in rodents [25]. As a result, studying the animals fed with HFD became an intriguing way to explore several features of NDDs. Indeed, even short-term exposure to HFD causes biological changes associated with NDDs.

Emerging evidence suggests that addressing a single metabolic pathway will be insufficient to slow the course of NDDs since many divergent components of brain metabolism are disrupted by AD and PD [26]. Therefore, focusing on the underlying mechanisms of AD and PD, including neuroinflammation, mitochondrial changes, and oxidative stress, may be a promising treatment approach. In our previous studies on metabolic diseases, we found that the level of glutathione (GSH) is not enough to maintain and regulate the thiol redox status of the liver [27,28]. Depleted liver GSH is restored by the administration of serine and *N*-acetylcysteine. Moreover, L-carnitine and nicotinamide riboside that both stimulate the transfer of fatty acids from cytosol to mitochondria have been identified as two additional cofactors that are depleted in patients with metabolic disorders [28].We developed combined metabolic activators (CMA) consisting of L-serine, *N*-acetyl cysteine (NAC), nicotinamide riboside (NR), and L-carnitine tartrate (LCAT, the salt form of L-carnitine) based on integrative network analysis of non-alcoholic fatty liver disease multi-omics data and demonstrated that CMA administration stimulates mitochondria, accelerates fatty acid oxidation and reduces inflammatory markers in both animals and humans [27,29–33]. Recently, we generated liver transcriptomics data in NAFLD hamster model and analysed the data using a hepatocyte-specific genome-scale metabolic model. We systemically determined the molecular changes after the supplementation of CMA and found that it activates mitochondria in the liver tissue by modulating global lipid, amino acid, antioxidant and folate metabolism [34]. Furthermore, CMA improved plasma levels of metabolites linked with antioxidant metabolism and inflammatory proteins in COVID-19 patients compared to the placebo [32].

Due to the metabolic abnormalities associated with the progression of AD and PD, we hypothesized that the treatment of patients with CMA might activate the mitochondria in the brain and other tissues and improve the metabolic health of NDDs patients. For this aim, we initially analysed brain transcriptomics data from 629 AD patients and 704 control participants through the use of genome-scale metabolic models. Next, we investigated the effect of CMA administration on the metabolic, behavioural and histological parameters associated with the NDDs in the animal models.

2. Material and methods

2.1. Transcriptomics data analysis of the brain in AD patients

The mRNA expression profiles of 629 AD and 704 age–, gender– and postmortem interval–matched control samples were obtained from the Religious Orders Study and Rush Memory Aging Project (ROSMAP) datasets [35–37]. The data has been normalized by quantile scaling, TMM normalization and Pareto scaling. Batch removal was performed using Limma *removeBatchEffect* [38], using experiment number as the batch variable. Quality control was confirmed by t-SNE. No samples were excluded due to low quality. DESeq2 [39] was used to identify the DEGs with uniform size factors. Ensembl Biomart [40] was used to map different gene accession IDs or symbols. Gene set enrichment (GSE) was performed by using *piano* [41]. The top 5 % DEGs by DESeq2 statistic were accepted for GSE analysis (Dataset S1). To identify the significantly changed metabolites in AD, we performed the Reporter metabolite analysis based on the RAVEN Toolbox 2.0 *reporterMetabolites* function [42], which uses DEGs information through the network topology of the reference metabolic model. The *iBrain2845* [43] genome-scale metabolic model was used as the reference metabolic model. KEGG Pathway Mapper [44] was used to identify predicted changed pathways based on

maps M01200, M01212, and M01230.

2.2. Animal study design for AD

12-week-old female albino Sprague-Dawley rats (weighing 320-380 g) were kept at a controlled temperature of 22 ± 2 °C and a controlled humidity of 50 ± 5 % on a 12-hour light/dark cycle in cages. Food and water were available ad libitum. The exclusion criteria were if rats experienced reduced appetite, pain or other symptoms with conflicts with animal ethics, as assessed by a veterinarian. The animal experiments are performed at Medical Experimental Research Center, Atatürk University, Erzurum, Turkey. Investigators, pathologists and statistician were blinded to the study design. All experiments for the treatment of the animals were approved by the Ethics Committee of Atatürk University (Atatürk University Experimental Research Center, Erzurum, Turkey, 31.05.2022/No:103), and were conducted following the National Institutes of Health Guide for Care and Use of Laboratory Animals.

2.2.1. CMA administration to animals to the metabolic AD-like model

After acclimation to laboratory conditions for 1 week, rats were divided into two groups using a completely randomized design. The primary outcome measure is the efficacy of CMA and individual components on brain and liver tissues of the streptozotocin (STZ) induced AD-like animal model by measuring pathological changes. Groups received dietary regimens of either a Chow diet (Group 1–2, CD) or a high-fat diet (Group 3–10, HFD) for 5 weeks. Group 2 (n = 4) were fed with CD and treated with STZ. The animals in Group 3 (n = 4) were fed with HFD for 3 weeks and sacrificed to verify the model development. Groups 4–10 were fed with HFD for 5 weeks. In total 37 rats were included in the study. Group 1 was the control group of the HFD, Group 4 was the control group for drug studies. After 3 weeks, the animals in Groups 5–10 were treated with STZ and administered with individual or combined metabolic activators, including L-serine, NAC, LCAT and NR for 2 weeks. Group 5, treated only with STZ; Group 6, treated with STZ and serine (1000 mg/kg once daily by oral gavage); Group 7, treated with STZ and NAC (300 mg/kg once daily by oral gavage); Group 8, treated with STZ and LCAT (100 mg/kg once daily by oral gavage); Group 9, treated with STZ and NR (120 mg/kg once daily by oral gavage); Group 10, treated with STZ and serine (1000 mg/kg once daily by oral gavage), NAC (300 mg/kg once daily by oral gavage), LCAT (100 mg/kg/day) and NR (120 mg/kg once daily by oral gavage).

The body weight of the rats was recorded each week (Dataset S2). After 5 weeks, all animals were anesthetized with isoflurane and sacrificed. Blood samples were collected from the abdominal aorta and centrifuged at 8000 rpm for 15 min at 4 °C for blood biochemistry analysis using an automatic chemical analyser. The internal organs, including the heart, adipose tissues, liver, kidney, brain, muscle, intestine (duodenum, ileum, jejunum), pancreas, colon and stomach were immediately removed, snap-frozen in liquid nitrogen and stored at −80 °C.

2.2.2. Intracerebroventricular-streptozotocin (STZ) injection

Before surgical procedures, the rats were anesthetized by intraperitoneal administration of ketamine–xylazine (50 mg/kg ketamine and 5 mg/kg xylazine) and placed individually in the stereotaxic instrument (Stoelting, Illinois, USA). Stereotaxic coordinates for injection were 0.8 mm posterior to the bregma, 1.5 mm lateral to the sagittal suture and 3.6 mm below the brain surface [45]. Then, 10 μl of STZ (3 mg/kg, Sigma-Aldrich, Darmstadt, Germany) were injected over 3 min with a Hamilton micro-syringe into the bilateral ventricle. The injection needles were left in place for an additional 2 min to allow diffusion.

2.2.3. Immunohistochemical examination

Liver (acinar region) and brain (cerebral cortex) tissue samples obtained as a result of the experimental procedure were fixed in 10 % buffered formalin solution for 48 h. Following the routine tissue procedure, the tissues were embedded in paraffin blocks and 4 μm thick sections were taken from each block. Preparations prepared for histopathological examination were stained with Haematoxylin-Eosin (HE) and examined with a light microscope (Olympus BX51, Germany). According to histopathological findings sections were evaluated by two independent pathologists as none (−), very mild (+), mild (++), moderate (+++) and severe (++++). Definition of histopathological scale is presented in Dataset S2.

Tissue sections taken on adhesive (poly-L-Lysin) slides for immunoperoxidase examination were deparaffinized and dehydrated. After washing the tissues with suppressed endogenous peroxidase activity in 3 % H_2O_2 were boiled in antigen retrieval solution. In order to prevent nonspecific background staining in the sections, protein block compatible with all primary and secondary antibodies was dropped and incubated for 5 min. Caspase 3 (cat no:sc-56053 dilution ratio:1/100 US) for liver tissues and 8-OHdG (Cat no: sc-66036 dilution ratio: 1/100 US) for brain tissues was used as the primary antibody. 3-3′ Diaminobenzidine (DAB) chromogen was used as chromogen. Sections were examined under fluorescent microscope (ZEISS Germany) and were evaluated in the ZEISS Zen Imaging Software program according to the manufacturer recommendations.

2.2.4. Immunofluorescence examination

Tissue sections taken on adhesive (poly-L-Lysin) slides for immunoperoxidase examination were deparaffinized and dehydrated. After washing the tissues with suppressed endogenous peroxidase activity in 3 % H_2O_2 were boiled in antigen retrieval solution. In order to prevent nonspecific background staining in the sections, protein block compatible with all primary and secondary antibodies was dropped and incubated for 5 min. For liver tissues, primary antibody 8-OHdG (Cat No: sc-66036 Dilution Ratio:1/100 US) was dropped and incubated at 37 °C for 1 h. After washing, secondary FITC (Cat No: ab6717 Dilution Ratio:1/500 UK) was dropped and incubated at 37 °C for 30 min.

The other primary antibody H2A.X (Cat No: I 0856-1 Dilution Ratio:1/100 US) was dropped and incubated at 37 °C for 1 h. After washing, secondary Texas Red (Cat No: sc-3917 Dilution Ratio:1/100 US) was dropped and incubated at 37 °C for 30 min. DAPI (Cat No:D-1306 Dilution Ratio:1/200 US) was dripped onto the washed tissues and incubated in the dark for 5 min, then glycerine was sealed.

For brain tissues, primary antibody Caspase 3 (Cat No:sc-56053 Dilution Ratio:1/100 US) was dropped and incubated for 1 h at 37 °C. After washing, secondary FITC (Cat No: ab6717 Dilution Ratio:1/500 UK) was dropped and incubated at 37 °C for 30 min. The other primary antibody H2A.X (Cat No:I 0856-1 Dilution Ratio:1/100 US) was dropped and incubated at 37 °C for 1 h. After washing, secondary Texas Red (Cat No: sc-3917 Dilution Ratio:1/100 US) was dropped and incubated at 37 °C for 30 min. DAPI (Cat No:D-1306 Dilution Ratio:1/200 US) was dripped onto the washed tissues and incubated in the dark for 5 min, then glycerine was sealed. Sections were examined under fluorescent microscope (ZEISS Germany) and were evaluated in the ZEISS Zen Imaging Software program according to the manufacturer recommendations.

2.3. Animal study design for PD

12-week-old female Wistar rats weighing 320–380 g were utilized and housed at a regulated temperature of 22 ± 2 °C and a controlled humidity of 5 % on a 12-hour light/dark cycle in cages. Food and water were available ad libitum. The Ethics Committee of Atatürk University authorized all animal treatment studies (Atatürk University Experimental Research Center, Erzurum, Turkey, 31.05.2022/No:103), which were carried out in line with the National Institutes of Health Guide for the Care and Use of Laboratory Animals. Investigators, pathologists and statistician were blinded to the study design. The exclusion criteria were if rats experienced reduced appetite, pain or other symptoms with conflicts with animal ethics, as assessed by a veterinarian. 6-

hydroxydopamine hydrochloride (6-OHDA, CAS No. 28094-15-7), ascorbic acid (L-ascorbic acid, CAS No. 50-81-7) and apomorphine hydrochloride (CAS No. 413-20-7) were obtained from Sigma-Aldrich Co. LLC (Germany). High-fat feed was obtained from HEKA Science (Istanbul, Turkey).

After a week of acclimating to laboratory settings, rats were divided into two groups using a completely randomized design. The primary outcome measure is the efficacy of CMA and individual components on brain and liver tissues of the 6-hydroxydopamine (6-OHDA) induced PD-like animal model by measuring pathological changes and behavioural tests. Groups that received dietary regimens received either CD or HFD. Animals in Group 1 (n = 3) were fed with standard CD for 4 weeks; Group 2 (n = 3) were fed with CD and treated with 6-OHDA. Animals in Group 3 (n = 3) were fed with HFD for 4 weeks. Animals in Group 4 (n = 3) were fed with HFD and treated with 6-OHDA. In total 37 rats were included in the study. Group 1 was the control group of the HFD, Group 4 was the control group for drug studies. Animals in Groups 5–10 were fed with HFD and treated with 6-OHDA. After 2 weeks, the animals in Groups 5–10 administered with CMA and its individual components including L-serine (9.50 mmol/kg/day), NAC (1.84 mmol/kg/day), L-CAT, (0.62 mmol/kg/day) and NR (0.41 mmol/kg/day) for 2 weeks. The orogastric applications were made until the sacrification process.

2.3.1. 6-OHDA lesion models of PD in rats

The 6-OHDA lesion was performed according to the previous literature [46,47]. Briefly, following anaesthesia by intraperitoneal injection of ketamine/xylazine (10/60 mg/kg b.w.), rats were positioned into a stereotaxic frame (Stoelting, Illinois, USA). The 6-OHDA was then injected into the right side of the skull using a stainless-steel needle. According to Paxinos and Watson [48], the needle point was inserted 4.5 mm posterior to the bregma, 1.2 mm lateral to the sagittal suture, and 9 mm ventral to the skull surface. Then, 6-OHDA (8 μl/4 μl in saline with 0.01 % ascorbic acid) was injected over 4 min, with the needle kept in place for another 4 min to avoid backflow.

2.3.2. Behavioural test in the PD-like animal model

Animals were tested for locomotor activity and apomorphine-induced rotation by an investigator blind to the treatment protocols. The locomotor activity was measured using a Plexiglas square (40 × 40 cm) with 40 cm high walls, equipped with a video-tracking system (ACT 508 Activity Meter, Commat LTD, Ankara, Turkey) as described previously [49]. The rats were introduced individually in the middle of a square arena and followed for 5 min. The crossed squares, pauses, and animal raising (vertical activity) were all recorded.

Apomorphine administration causes aberrant contralateral rotations in PD-like model rats [50,51]. Apomorphine HCl was given to the rats at a 2.5 mg/kg dosage intraperitoneally. Five minutes after the administration, the animals were individually placed into open-top square cages with a 40 cm diameter. The counter-clockwise (contralateral) rotations were recorded for 30 min, and the number of apomorphine-induced rotations was counted.

2.3.3. Immunohistochemical examination

Liver (acinar region) and brain (substantia nigra) tissue samples obtained as a result of the experimental procedure were fixed in 10 % buffered formalin solution for 48 h. Following the routine tissue procedure, the tissues were embedded in paraffin blocks and 4 μm thick sections were taken from each block. Preparations prepared for histopathological examination were stained with Haematoxylin-Eosin (HE) and examined with a light microscope (Olympus BX51, Japan). According to histopathological findings sections were evaluated by two independent pathologists as none (−), very mild (+), mild (++), moderate (+++) and severe (++++). Definition of histopathological scale is presented in Dataset S2.

Tissue sections taken on adhesive (poly-L-Lysin) slides for immunoperoxidase examination were deparaffinized and dehydrated. After washing the tissues with suppressed endogenous peroxidase activity in 3 % H_2O_2 were boiled in antigen retrieval solution. In order to prevent nonspecific background staining in the sections, protein block compatible with all primary and secondary antibodies was dropped and incubated for 5 min. For brain tissue 8-OHdG (cat no:sc-66036 dilution ratio:1/100 US), for liver tissues JNK1/3 (cat no:sc-514539 dilution ratio:1/100 US) was used as the primary antibody. 3-3′ Diaminobenzidine (DAB) chromogen was used as chromogen. Sections were examined under fluorescent microscope (ZEISS Germany) and were evaluated in the ZEISS Zen Imaging Software program according to the manufacturer recommendations.

2.3.4. Immunofluorescence examination

Tissue sections taken on adhesive (poly-L-Lysin) slides for immunoperoxidase examination were deparaffinized and dehydrated. After washing the tissues with suppressed endogenous peroxidase activity in 3 % H_2O_2 were boiled in antigen retrieval solution. In order to prevent nonspecific background staining in the sections, protein block compatible with all primary and secondary antibodies was dropped and incubated for 5 min. For liver tissues, primary antibody 8-OHdG (Cat No: sc-66036 Dilution Ratio:1/100 US) was dropped and incubated at 37 °C for 1 h. After washing, secondary FITC (Cat No: ab6717 Dilution Ratio:1/500 UK) was dropped and incubated at 37 °C for 30 min. The other primary antibody H2A.X (Cat No:I 0856-1, Dilution Ratio:1/100 US) was dropped and incubated at 37 °C for 1 h. After washing, secondary Texas Red (Cat No: sc-3917 Dilution Ratio:1/100 US) was dropped and incubated at 37 °C for 30 min.

For brain tissue, primary antibody NeuN (Cat No: ab104225, Dilution Ratio:1/100 UK) was dropped and incubated at 37 °C for 1 h. After washing, secondary FITC (Cat No: ab6717 Dilution Ratio:1/500 UK) was dropped and incubated at 37 °C for 30 min. The other primary antibody Caspase 3 (Cat No: sc-56053 Dilution Ratio:1/100 US) was dropped and incubated at 37 °C for 1 h. After washing, secondary Texas Red (Cat No: ab6719, Dilution Ratio:1/500 UK) was dropped and incubated at 37 °C for 30 min. DAPI (Cat No:D-1306 Dilution Ratio:1/200 US) was dripped onto the washed tissues and incubated in the dark for 5 min, then glycerin was sealed. Sections were examined under fluorescent microscope (ZEISS Germany) and were evaluated in the ZEISS Zen Imaging Software program according to the manufacturer recommendations.

2.4. Statistical analysis

Data are shown as mean ± standard deviation (SD) for continuous variable. Data distribution was tested for normality by the Shapiro–Wilk test. One-way ANOVA was used for continuous variables with a normal distribution and the Mann–Whitney-*U* test for variables with a non-normal distribution. Statistical significance was considered when p-value <0.05. Statistical sample size predetermination was not carried out. All analyses were done by R (version, 4.1.3).

3. Results

3.1. Analysis of transcriptomics data reveals mitochondrial dysfunction in the brain of AD patients

We obtained the global mRNA expression profiling of 629 AD patients and 704 controls from the Religious Orders Study/Memory and Aging Project (ROSMAP) [35–37]. The mean age was 87.8 ± 3.6 years for AD patients and 85.3 ± 5.1 years for controls. The AD group was 65.2 % female, 97.3 % white, and had a mean postmortem interval of 6.95 ± 4.29 h. The control group was 68.2 % female, 97.6 % white, and had a mean postmortem interval of 7.95 ± 6.80 h. The AD group had a mean Mini Mental State Examination (MMSE) result of 13.7 ± 8.3 and 36.4 % of individuals had at least one ApoE4 allele. For the control group, the mean MMSE result was 28.3 ± 1.5 and 18.0 % had at least one ApoE4 allele.

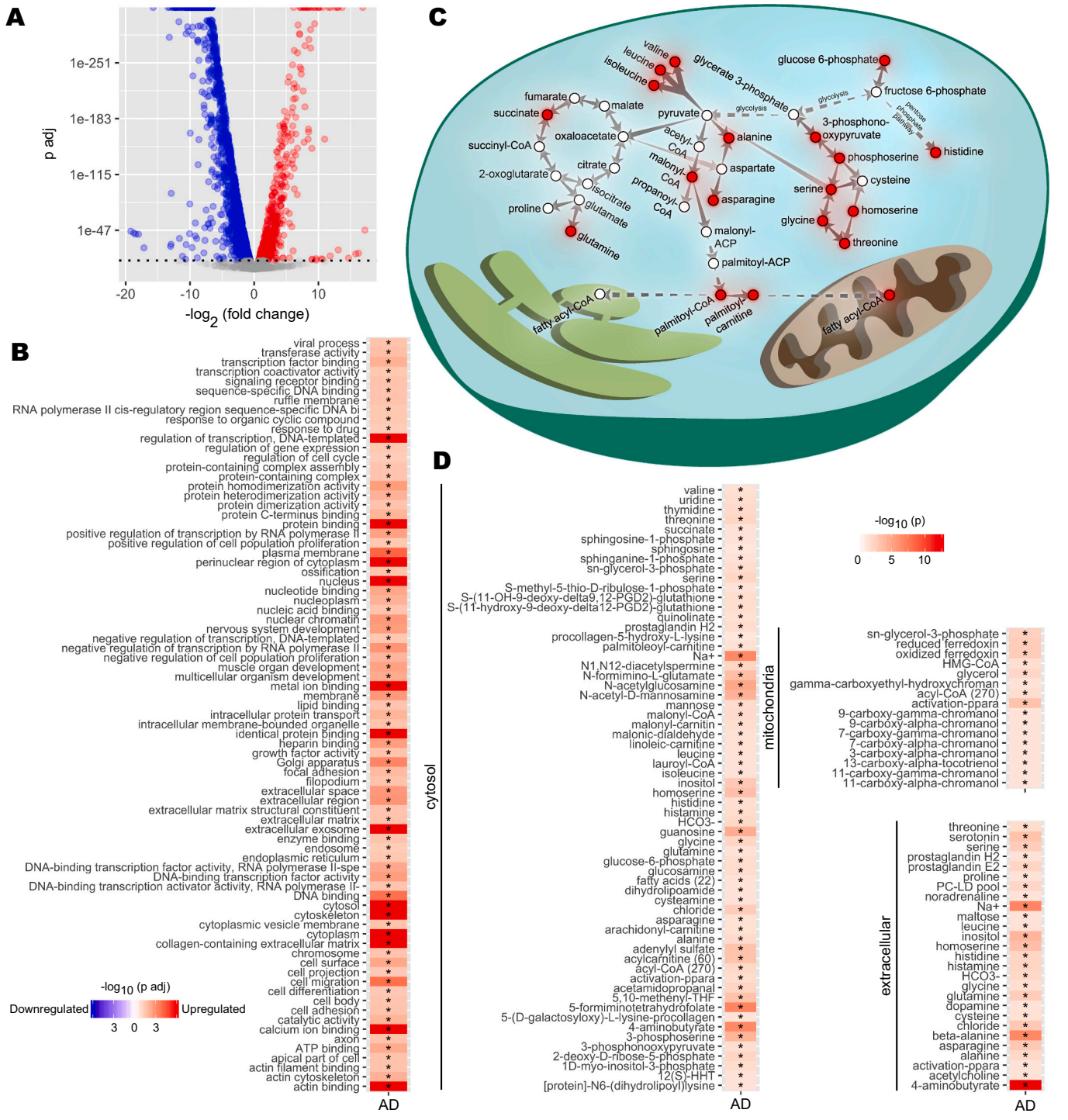

Fig. 1. Transcriptomic analysis of brain tissue samples from AD patients.
A) Differential expression analysis for AD brain samples compared to healthy controls was performed. DEGs were determined from gene expression values. DEGs with a p-value of 1 × 10–10 or smaller after Benjamini-Hochberg adjustment were determined statistically significant. Each point represents one gene. Red, significantly upregulated genes; blue, significantly downregulated genes; grey, not significant. **B)** Functional enrichment analysis was performed. Gene set enrichment analysis was applied to the DEGs to determine upregulated and downregulated GO terms compared to controls. The colour scale indicates the direction of enrichment and p-value after Benjamini-Hochberg adjustment. Significance code: *, Adj.p < 0.05. **C)** Carbon metabolism pathway analysis. Alterations to pathways were inferred from reporter metabolite analysis. Key reactions and pathways linking reporter metabolites (red nodes) are shown. Reactions are simplified and arrows may represent multiple reactions. D) Reporter metabolite analysis. Statistics from DEG analysis were used to infer altered metabolites based on the iBrain2845, a functional genome-scale metabolic model of the brain. Asterisks indicate statistical significance based on Student's *t*-test. p value <0.05. (For interpretation of the references to colour in this figure legend, the reader is referred to the web version of this article.)

Based on brain transcriptomics data, we performed differential expression analysis and identified 914 significantly (p-adjusted <1.0 E-10) upregulated and 1725 significantly (p-adjusted <1.0 E-10) downregulated differentially expressed genes (DEGs) (Fig. 1A, Dataset S1). We identified several upregulated metabolism-related genes, including pyruvate dehydrogenase kinase 4 (PDK4), carnitine palmitoyl transferase (CPT1A), hexokinase 2 (HK2), and spermine oxidase (SMOX), as well as downregulated genes including acyl-CoA dehydrogenases (ACADs), ATP synthase (ATP5MGL), and acetyl- and acyltransferases (GCNT7, MBOAT4, GALNT17). These results suggest that metabolic alterations in glycolysis, fatty acid biogenesis and the urea cycle are critical for AD patients.

GSE analysis revealed enrichment of cytoskeleton- and neuron-related GO terms and suggested widespread perturbations to diverse metabolic pathways in the cytosol and mitochondria in AD compared to control. (Fig. 1B, Dataset S1). Then, we performed reporter metabolite analysis to predict the significantly changed metabolites in each subcellular compartment using a genome-scale metabolic model of brain tissue [43,52]. We identified numerous reporter metabolites related to glycolysis, amino acid metabolism (e. g. glycine, serine, threonine, alanine and branched-chain amino acid valine, leucine and isoleucine), mitochondrial metabolism (acyl-CoA and ferredoxin) and TCA cycle (e. g. succinate and glutamine) (Fig. 1C and D, Dataset S1). These results suggested a widespread perturbation in energy metabolism-related to brain cell survival and mitochondrial dysfunction in the brain.

3.2. Administration of CMA to a metabolic model of Alzheimer's disease

To test the effect of CMA administration in animals, we administered CMA and individual metabolic activators to the rat model of AD, developed after intracerebroventricular-streptozotocin (STZ) injection. We observed that administration of all constituents of CMA (in combination or separately) significantly ($p < 0.05$) decreased the plasma levels of triglycerides (TG) compared to the control group (Group 4; Fig. 2A&B, Dataset S2). In parallel, administration of only serine or NR significantly decreased total cholesterol ($p = 0.01$) and low-density lipoprotein (LDL; $p = 0.03$) in rats (Fig. 2B, Dataset S2). Additionally, a significant reduction in total cholesterol ($p = 0.04$) and LDL ($p = 0.03$) was observed in NAC-treated and LCAT-treated rats, respectively (Fig. 2B, Dataset S2). Of note, we found significant reductions in plasma AST ($p = 0.03$) and an increase in plasma ALP ($p = 0.04$) concentrations only in LCAT-treated rats (Fig. 2B, Dataset S2).

Additionally, the histological analyses and immunofluorescence imaging techniques showed significant neuronal tissue damage in the high-fat diet (HFD) and HFD + STZ groups' brains compared to those fed with the CHOW diet (Figs. 2C & 3, Dataset S2). Specifically, animals fed by HFD for five weeks developed more hyperemia as well as more degeneration and necrosis in neurons (Figs. 2C & 3, Dataset S2). In parallel, DNA damage markers (namely 8-OHdG and H2A.X) and caspase 3 were elevated in the HFD groups (Figs. 2C & 3, Dataset S2). These animal models allowed us to examine each rat group's histopathological differences and assess the brain tissue response to CMA administration compared to the HFD + STZ group (Figs. 2C & 3, Dataset S2). We observed that hyperemia, degeneration and necrosis in neurons were improved by individual serine, LCAT, or NR supplementation as well as by their combination. However, we observed a better improvement after CMA administration than individual metabolic activators. These findings were also supported by immunohistochemical evidence of decreased immunoreactivity seen in neurons (Figs. 2C & 3, Dataset S2). Notably, rats receiving CMA therapy developed less hyperemia in brain tissue and very mild necrosis in neurons (Figs. 2C & 3, Dataset S2). In parallel to the improvement in the brain, we also observed dramatic improvement in the liver after the administration of CMA. Scoring of histopathological, immunohistochemical and immunofluorescence findings for brain and liver tissues are presented in Fig. 2C.

3.3. Administration of CMA shows a beneficial effect on behavioural functions in PD rats

After a week of acclimating the rats to laboratory settings, we randomly assigned animals to one of two dietary regimens: 8 animals fed with a standard CHOW diet (CD) and 32 animals fed with a high-fat diet (HFD) for 2 weeks. After 2 weeks, 4 animals fed with CD and 28 animals fed with HFD were treated with 6-hydroxydopamine (6-OHDA). 24 animals fed with HFD also administered with CMA and its individual components, including L-serine (9.50 mmol/kg/day), NAC (1.84 mmol/kg/day), L-CAT, (0.62 mmol/kg/day) and NR (0.41 mmol/kg/day) for 2 weeks (Fig. 4A). The orogastric applications were made until the scarification process. During the 4-weeks study, we did not observe any significant differences in the bodyweight of animals fed with HFD (Fig. 4B).

We performed a biochemistry examination of metabolic parameters. We found that bilirubin, aspartate aminotransferase (AST), low-density lipoprotein (LDL), total protein and white blood cell levels were significantly decreased, but alanine transferase (ALT), creatinine, glucose, hemoglobin and hematocrit levels were significantly increased between treated groups (administered with individual or CMA) and HFD plus 6-OHDA group (Fig. 4C). Our animal study showed that CMA administration improved the neurological behaviour of the animals together with the global metabolic parameters.

Contralateral rotation was detected in the animals fed with HFD but not in the animals fed with CD. When animals were given dopaminergic agents after a unilateral lesion was created with 6-OHDA treatment, they exhibited rotational behaviours and similar movements. Contralateral rotations were detected on average as 303.33 in the HFD + 6-OHDA group, while 6-OHDA alone was 183.33. We observed that the administration of the individual metabolic activators improved the contralateral rotation of the animals, whereas the CMA had a better effect compared to individual metabolic activators except for NR supplementation.

The motor functions of the animals were analysed by the locomotor activity test. In this context, the stereotypical, ambulatory, resting time percentage (resting) and distance travelled movements, as well as *horizontal and vertical activities* were evaluated (Fig. 5A & B). Stereotypical movement is defined as recognizing and grooming the animal's environment. A high value means that there is no restriction on the animal's movements. Ambulatory movement is all the walking movements of the animal on the ground without standing up. It is also expected to be high in animals whose motor functions function properly. Our observations revealed that CMA exhibited significantly ($p < 0.05$) ameliorated stereotypy compared to controls (Fig. 4C). The decreasing order of efficacy of treatment in ameliorating stereotypy was CMA > Serine + NAC + L-CAT > L-CAT > NR > NAC > Serine. Likewise, the supplementation with different individual metabolic cofactors or CMA ameliorated ambulatory activity. The percentage of resting time is directly related to ambulatory movement and occurs when animals with reduced motor activity tend to rest and remain still. The applications of 6-OHDA plus HFD- or only 6-OHDA in rats led to a statistically significant ($p < 0.05$) increase in time resting compared to control rats. The simultaneous treatment of individuals or CMA decreased the resting time (Table 1 & Fig. 5B).

Total distance defines the distance travelled by the subjects horizontally. An increase in the distance travelled indicates that the motor activity functions properly. Total distance in rats treated with CD plus 6-OHDA or HFD plus 6-OHDA was significantly decreased compared to animals fed with CD or HFD. Likewise, total distance amounts in the rats in which only serine was administered were lower than control values. However, the three combinations of metabolic activators or their individual administration (except serine) improved the total distance amounts and horizontal activity. In this regard, especially CMA administered rats displayed the best potency in enhancing the total distance travelled and horizontal activity (Table 1, Fig. 5A). In the

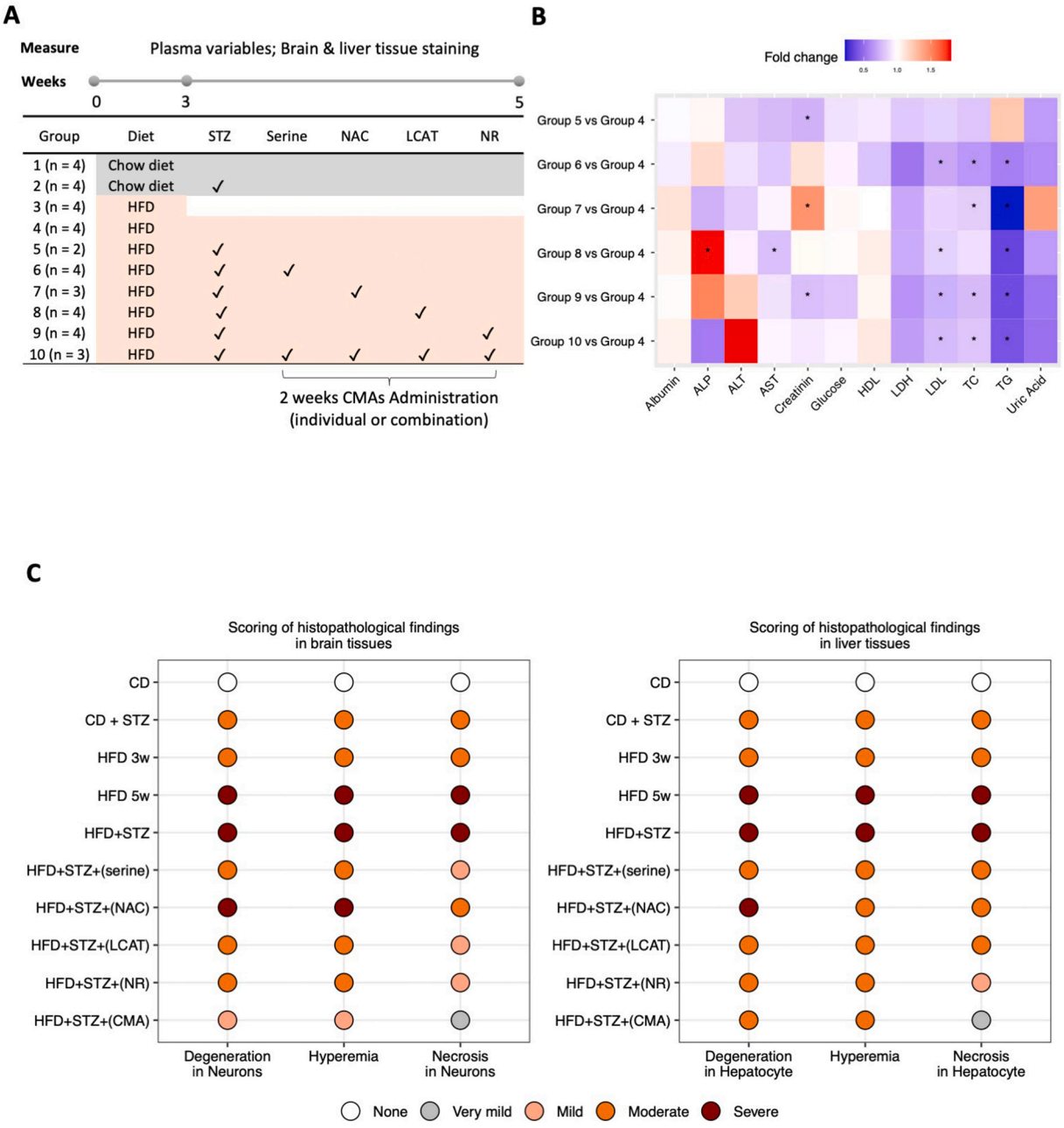

Fig. 2. The effect of CMA administration in AD-like animal model.
A) Rat animal groups in in vivo experiments. Group 1 (n = 4) were fed with only a regular Chow diet (CD) for 5 weeks; Group 2 (n = 4) were fed with CHOW and treated with streptozotocin (STZ). The remaining animals in Group 3 (n = 4) were fed with a high-fat diet (HFD) for 3 weeks and sacrificed to verify model development. Groups 4–10 were fed with HFD for 5 weeks. After 3 weeks, the animals in Groups 5–10 were treated with STZ and administered with individual or combined metabolic activators, including L-serine, NAC, LCAT and NR for 2 weeks. **B)** Heatmap shows FC based relative alterations of the clinical variables in the rat study groups. Asterisks indicate statistical significance based on one-way ANOVA or Mann–Whitney-*U* test, p-value <0.05 is considered as statistical significance. TG, triglyceride; TC, total cholesterol; ALP, Alkaline phosphatase; AST, Aspartate aminotransferase; ALT, Alanine aminotransferase; HDL, high-density lipoprotein; LDL, low-density lipoprotein; LDH, Lactate dehydrogenase. **C)** Histopathological images analysis results of rat brain (right side) and liver tissue (left side). Slides evaluated by two independent pathologists and immunopositivity scores were: None (−), very mild (+), mild (++), moderate (+++) and severe (++++).

locomotor activity test, the motor functions of the animals were tested, and the movements they made during the experiment were also shown with a diagram (Fig. 5A). In the diagram, the curiosity activities of the CMA-treated groups with excessive movements were continued, and it was revealed that they did not have anxiety (Fig. 5A).

3.4. Immunohistopathological examination of brain and liver tissues

Histopathological examination of brain tissues revealed that animals fed with HFD and treated with 6-OHDA had very severe degeneration, hyperemia and necrosis in the neurons. When the animals were administered with individual or CMA, mild degeneration and mild hyperemia were detected together with no necrosis in the neurons in the brain (Fig. 6). We also analysed the liver tissue of animals since we hypothesized that CMA improves the metabolic parameters, which may lead to improved neurological behaviours. Animals fed with HFD and treated with 6-OHDA had severe fatty degeneration and moderate hydropic degeneration in hepatocytes, as well as very severe hyperemia

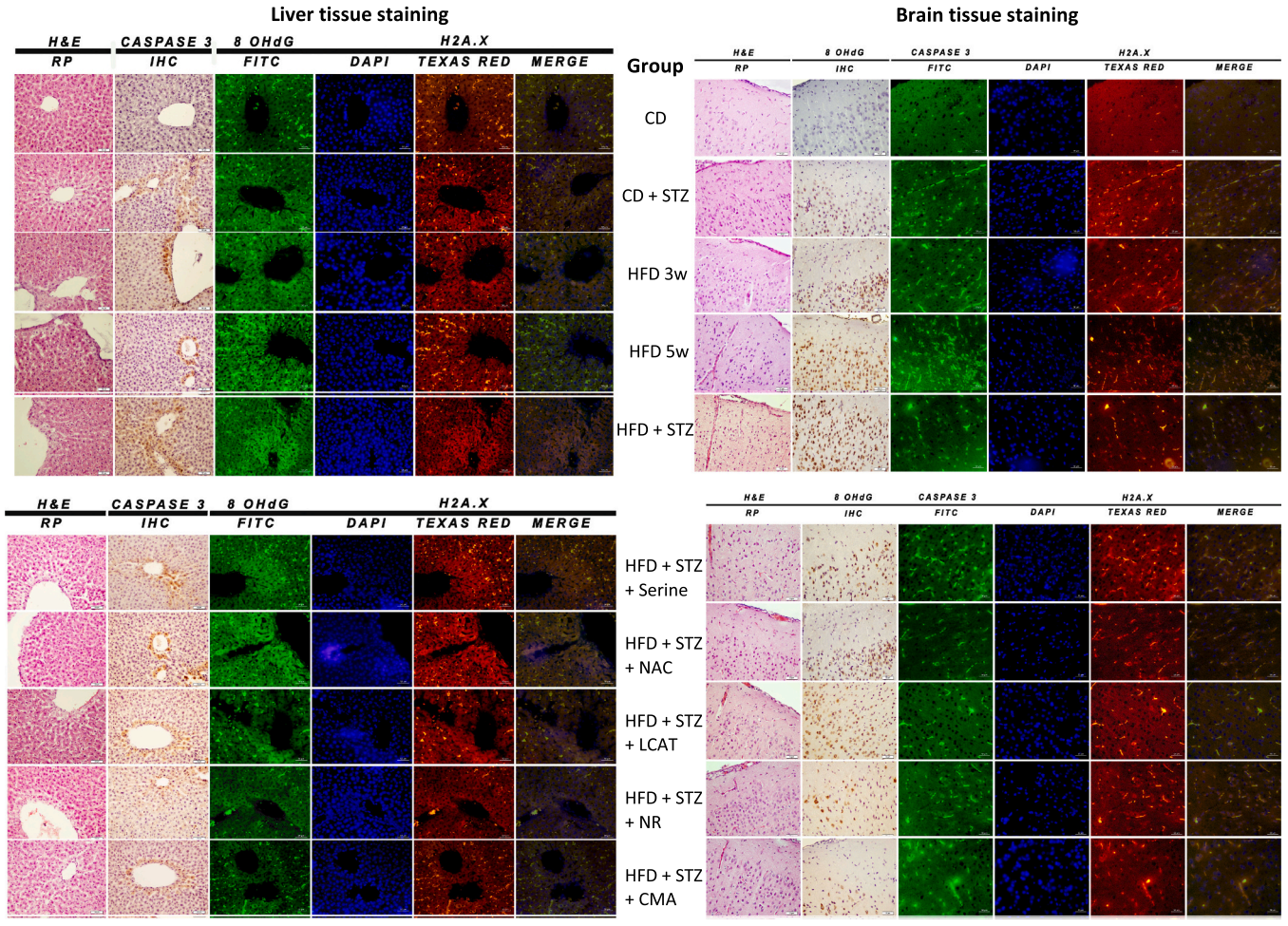

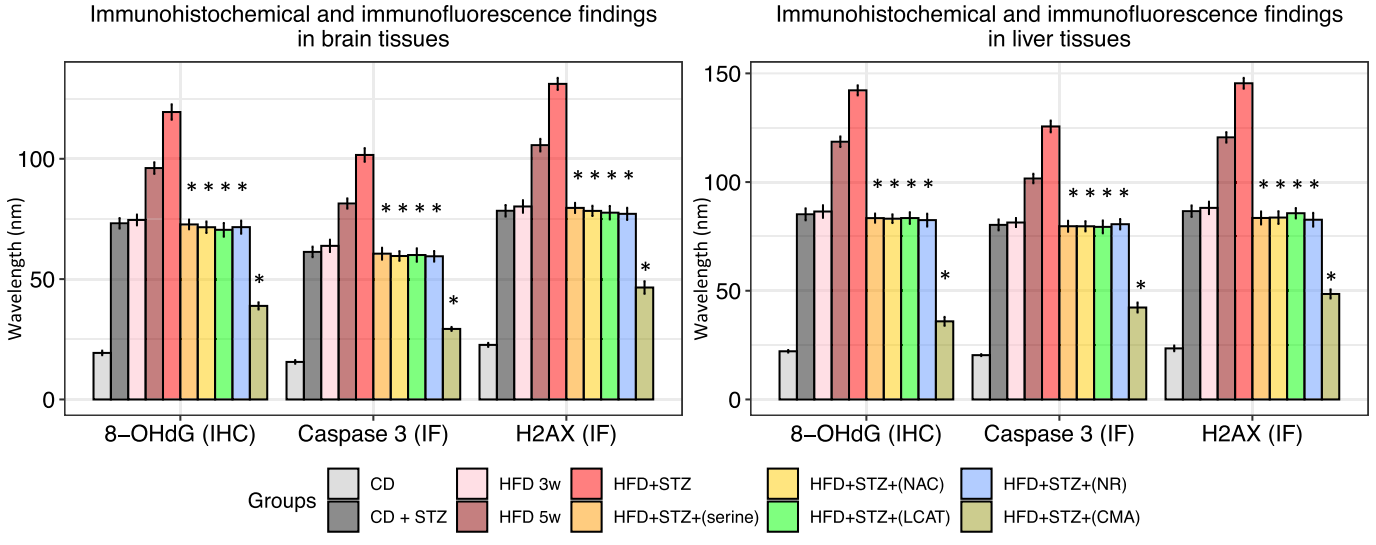

(caption on next page)

Fig. 3. Histopathological, immunohistochemical and immunofluorescence images of rat tissues in the AD like animal model. **A)** Histopathological (Haematoxylin &Eosin), immunohistochemical (Caspase 3 for liver, 8-OHdG for brain) and immunofluorescence (FITC, DAPI, Texas Red and merged) images of rat brain (antibodies: Caspase 3 and H2A.X) and liver (antibodies: 8-OHdG and H2A.X) tissues. Brain tissue (cerebral cortex) is presented at right side and liver tissue (acinar regions) at left side. Slides evaluated by two independent pathologists and histopathological scores were: None (−), very mild (+), mild (++), moderate (+++) and severe (++++). **B)** Bar plot shows immunohistochemical and immunofluorescent findings in rat brain (right side) and liver tissue (left side). Slides were evaluated by two independent pathologists. In order to determine the intensity of positive staining from the obtained images, 5 random areas were selected from each image. For immunohistochemical and immunofluorescent images, the positive/total area was calculated by measuring with the ZEISS Zen Imaging Software program. Data were statistically defined as mean and standard deviation (mean ± SD) for % area. CD: chow diet, OHDA: 6-hydroxydopamine hydrochloride, HFD: high-fat diet, NAC: *N*-acetyl-L-cysteine, LCAT: L-carnitine tartrate, NR: nicotinamide riboside, IF: Immunofluorescence, IHC: Immunohistochemistry. (For interpretation of the references to colour in this figure legend, the reader is referred to the web version of this article.)

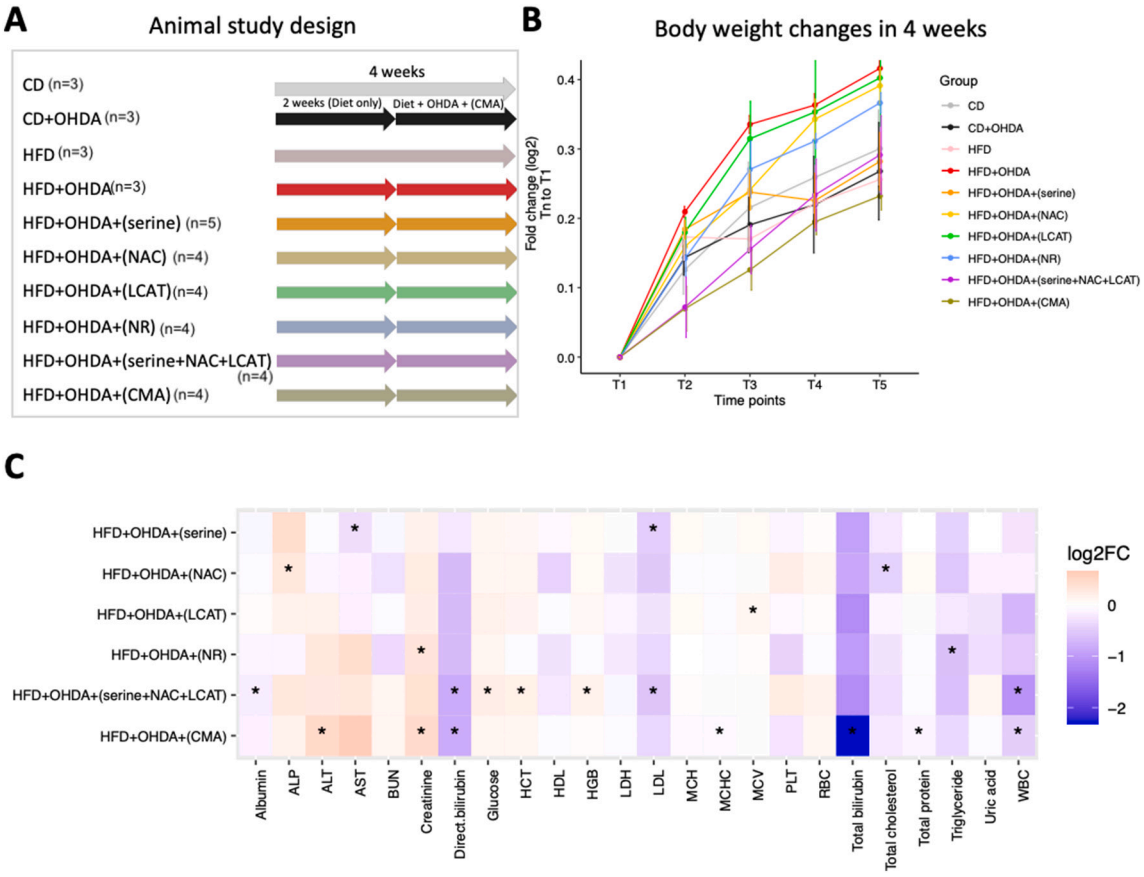

Fig. 4. Administration of CMA shows beneficial effect on plasma parameters in PD-like animal model.
A) Overview of the study design and group information. **B)** relative body weight changes of animals in each group within 4 weeks by comparing to the baseline. **C)** Heatmap plot shows log2FC of biochemical variables between treated groups (administered with individual or CMA) and HFD plus 6-OHDA group. Asterisk (*) denotes statistical significance ($p < 0.05$). The difference and p-value are estimated by one-way ANOVA or Mann–Whitney-*U* test. CD: chow diet, OHDA: 6-hydroxydopamine hydrochloride, HFD: high-fat diet, NAC: *N*-acetyl-L-cysteine, LCAT: L-carnitine tartrate, NR: nicotinamide riboside, ALP: alkaline phosphatase, ALT: alanine Aminotransferase, AST: aspartate transaminase, BUN: blood urea nitrogen, HCT: hematocrit, HDL: high-density lipoprotein, HGB: hemoglobin, LDH: lactate dehydrogenase, LDL: low-density lipoprotein, MCH: mean corpuscular hemoglobin; MCHC: mean corpuscular hemoglobin concentration, MCV: mean corpuscular volume, PLT: platelet (thrombocyte) count, RBC: red blood cell, WBC: white blood cell, log2FC: log transformation fold change. T1 represent 29th Sep 2021 and indicate the initial body weight of animals. T2 represent 6th Oct, 2021, T3 represent 13th Oct 2021, T4 represent 20th Oct 2021, and T5 represent 27th Oct 2021. (For interpretation of the references to colour in this figure legend, the reader is referred to the web version of this article.)

and mild necrosis in the vessels in the liver. After the administration of CMA and its individual components, we observed mild fatty degeneration and mild hydropic degeneration in hepatocytes, as well as mild hyperemia and no necrosis in the vessels in the liver (Fig. 7). A statistically significant difference ($p < 0.05$) was found compared with the HFD group treated with 6-OHDA.

Immunohistochemically examination of brain tissues in the animals fed with HFD and treated with 6-OHDA showed a very high expression of 8-OHdG, NeuN, Caspase 3 compared to animals fed with CD (Fig. 6). We examined the animals treated with individual or CMA immunohistochemically and observed a very mild 8-OHdG, cytoplasmic NeuN, Caspase 3 in the brain tissues of animals treated with CMA (Fig. 6). We found a statistically significant difference ($p < 0.05$) when comparing the animals administered with individual or CMA to the animals fed with HFD and treated with 6-OHDA. Similarly, we also immunohistochemically examined the liver tissues of the animals fed with HFD and treated with 6-OHDA and found that the expression of JNK, 8-OHdG, H2AX was significantly increased compared to control animals fed with CD (Fig. 7). After treating the animals with individual or CMA, we examined the liver tissues immunohistochemically and observed a very mild 8 JNK, 8-OHdG, H2AX expression in the liver tissue (Fig. 7). A statistically significant difference ($p < 0.05$) was found when comparing animals administered with individual or CMA to the animals fed with HFD and treated with 6-OHDA. Based on our analysis, we found

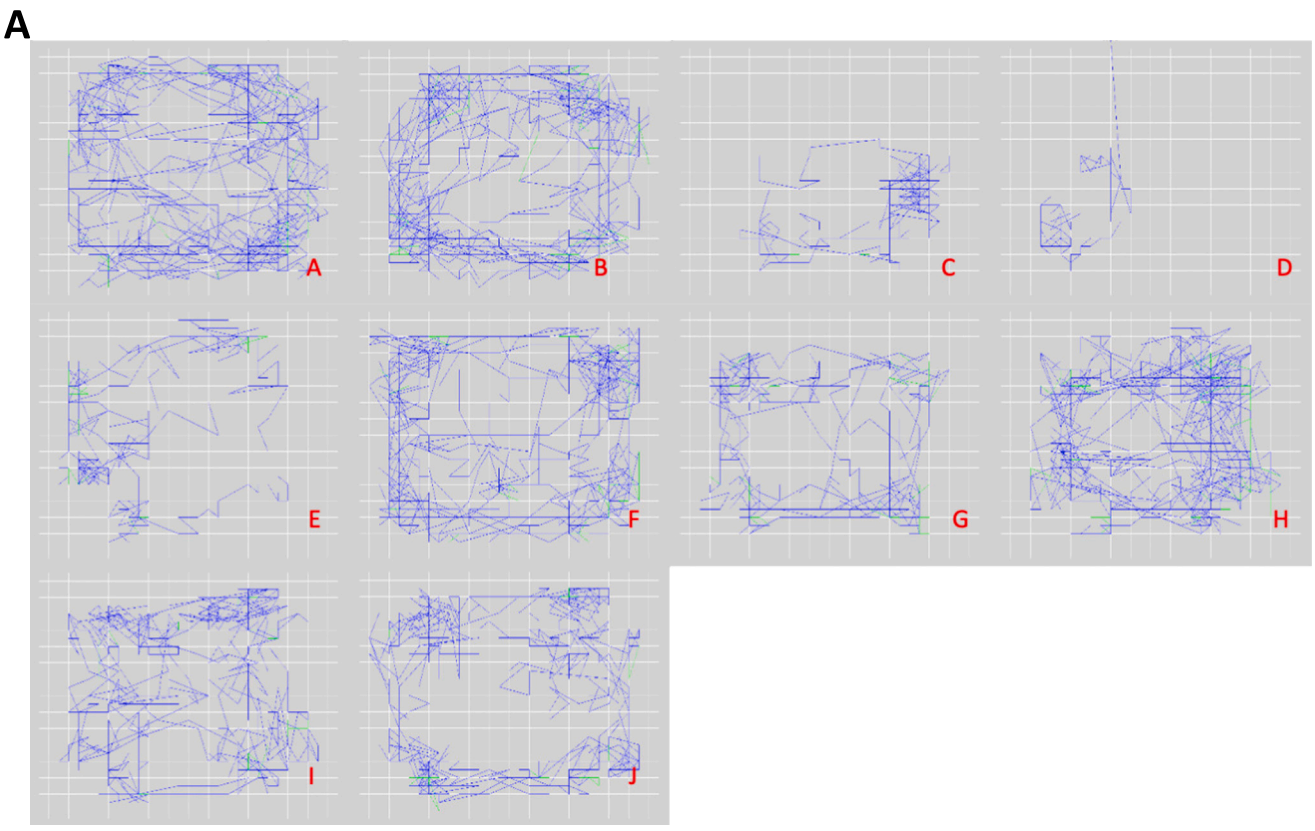

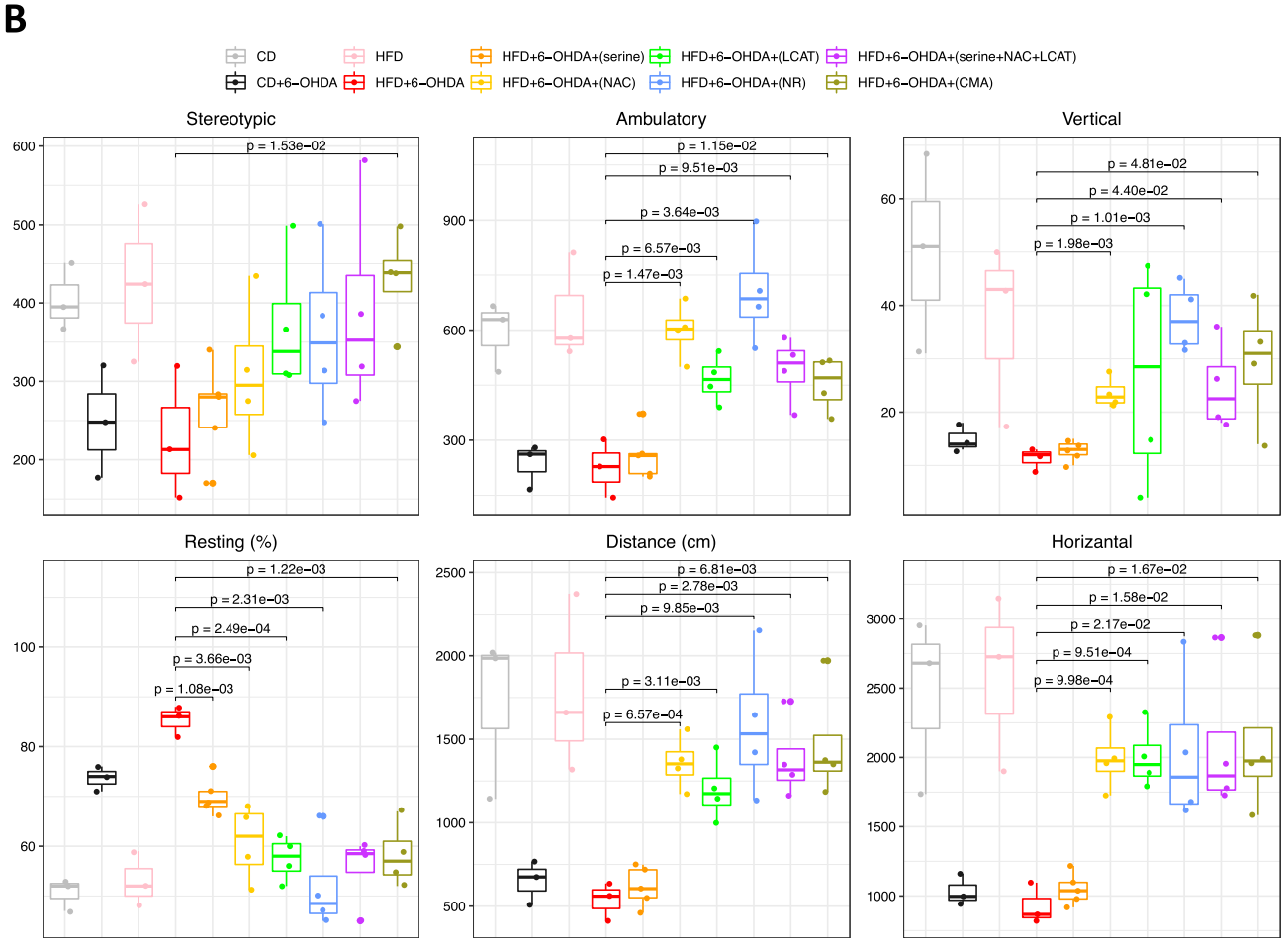

(caption on next page)

Fig. 5. Administration of CMA shows beneficial effect on behavioural functions in PD-like animal model. **A)** The activity meter graph consists of an image to represent the total locomotor activity of each treatment type. Different letters above the columns present significant differences ($p < 0.05$). **B)** Boxplot showing the changes of locomotor activity in each group. The comparison was applied between treated groups and HFD plus 6-OHDA group. **A**: CD, **B**: HFD, **C**: 6-OHDA, **D**: HFD + 6-OHDA, **E**: HFD + 6-OHDA + (serine), **F**: HFD + 6-OHDA + (NAC), **G**: HFD + 6-OHDA + (L-CAT), **H**: HFD + 6-OHDA + (NR), **I**: HFD + 6-OHDA + (serine + NAC + L-CAT), **J**: HFD + 6-OHDA + (CMA)**.** CD: chow diet, 6-OHDA: 6-hydroxydopamine hydrochloride, HFD: high-fat diet, NAC: *N*-acetyl-L-cysteine, LCAT: L-carnitine tartrate, NR: nicotinamide riboside.

Table 1
Comprehensive behavioural analysis of rats treated with HFD, 6-OHDA and different metabolic activators in the animal model of PD.

Groups	Stereotypic movement	Ambulatory movement	Vertical activity	Horizontal activity	Distance travelled (cm)	Resting (%)
CD	404.25 ± 42.70	593.75 ± 95.05	50.00 ± 18.50	24.50 ± 6.40	1715.50 ± 495.90	50.75 ± 3.20
HFD	425.00 ± 100.50	643.75 ± 146.05	36.75 ± 17.40	26.00 ± 6.30	1784.00 ± 537.20	53.00 ± 5.60
CD + 6-OHDA	248.25 ± 71.50	236.00 ± 61.30	15.00 ± 2.60	10.25 ± 1.30	650.00 ± 131.30	73.75 ± 2.50
HFD + 6-OHDA	228.25 ± 85.00	224.75 ± 79.05	11.25 ± 2.10	9.75 ± 1.50	536.00 ± 113.90	85.25 ± 3.10
HFD + 6-OHDA + (serine)	263.00 ± 62.70	260.75 ± 68.25*	12.75 ± 1.90	10.50 ± 1.20	616.75 ± 118.80	70.00 ± 3.80*
HFD + 6-OHDA + (NAC)	307.75 ± 96.05	598.00 ± 76.3*	23.75 ± 3.10*	19.75 ± 2.30*	1359.00 ± 159.80*	51.25 ± 4.70*
HFD + 6-OHDA + (L-CAT)	370.75 ± 89.60	466.00 ± 64.45*	27.00 ± 4.80	20.00 ± 2.30*	1199.25 ± 188.50*	57.50 ± 4.40*
HFD + 6-OHDA + (NR)	361.75 ± 108.10	704.75 ± 144.10*	37.75 ± 6.30*	20.50 ± 5.50*	1587.50 ± 429.20*	49.50 ± 11.40*
HFD + 6-OHDA + (serine + NAC + L-CAT)	390.50 ± 135.50	492.25 ± 90.05*	24.75 ± 8.30*	20.75 ± 5.30*	1380.25 ± 243.80*	55.50 ± 7.10*
HFD + 6-OHDA + (CMA)	429.75 ± 63.70*	453.75 ± 75.80*	29.50 ± 11.60*	21.00 ± 5.40*	1470.00 ± 343.80*	58.25 ± 6.50*

The difference between individual and combined metabolic activators-treated group and HFD plus 6-OHDA group. Statistical significance is derived from one-way ANOVA or Mann–Whitney-*U* test and Asterisk (*) denotes $p < 0.05$. CD: chow diet, 6-OHDA: 6-hydroxydopamine hydrochloride, HFD: high-fat diet, NAC: *N*-acetyl-L-cysteine, LCAT: L-carnitine tartrate, NR: nicotinamide riboside.

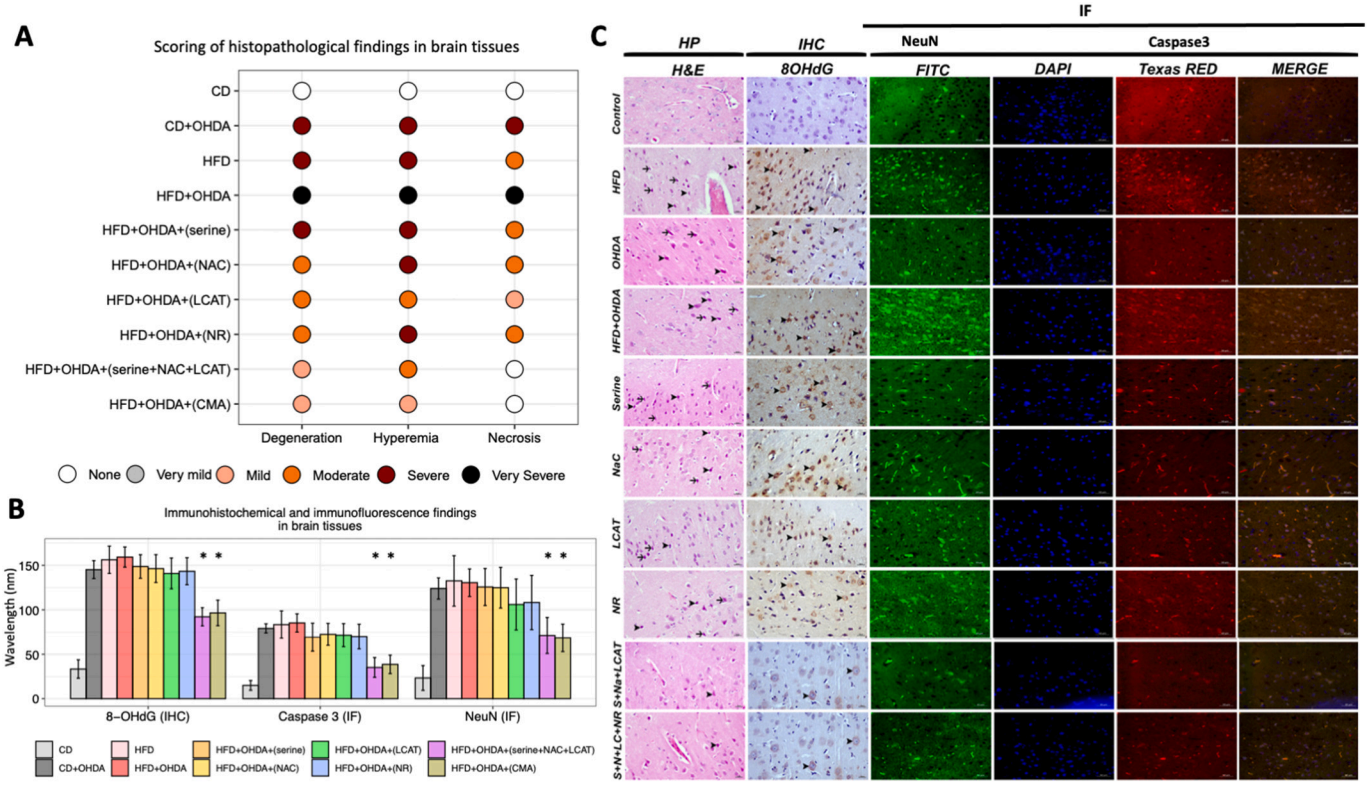

Fig. 6. Immunohistopathological examination of brain tissues in PD-like animal model.
A) Plot shows histopathological findings brain (cerebral cortex) tissues. **B)** Bar plot shows immunohistochemical and immunofluorescent findings in brain tissues. **C)** Histopathological (Haematoxylin &Eosin), immunohistochemical (8OHdG) and immunofluorescence (FITC, DAPI, Texas Red and merged) images of rat brain tissue (antibodies: Caspase 3 and NeuN). Slides evaluated by two independent pathologists. Histopathological scores were: None (−), very mild (+), mild (++), moderate (+++), severe (++++) and very severe (+++++). Slides evaluated by two independent pathologists. In order to determine the intensity of positive staining from the obtained images, 5 random areas were selected from each image. For immunohistochemical and immunofluorescent images, the positive/total area was calculated by measuring with the ZEISS Zen Imaging Software program. Data were statistically defined as mean and standard deviation (mean ± SD) for % area. CD: chow diet, 6-OHDA: 6-hydroxydopamine hydrochloride, HFD: high-fat diet, NAC: *N*-acetyl-L-cysteine, LCAT: L-carnitine tartrate, NR: nicotinamide riboside, IF: Immunofluorescence, IHC: Immunohistochemistry. (For interpretation of the references to colour in this figure legend, the reader is referred to the web version of this article.)

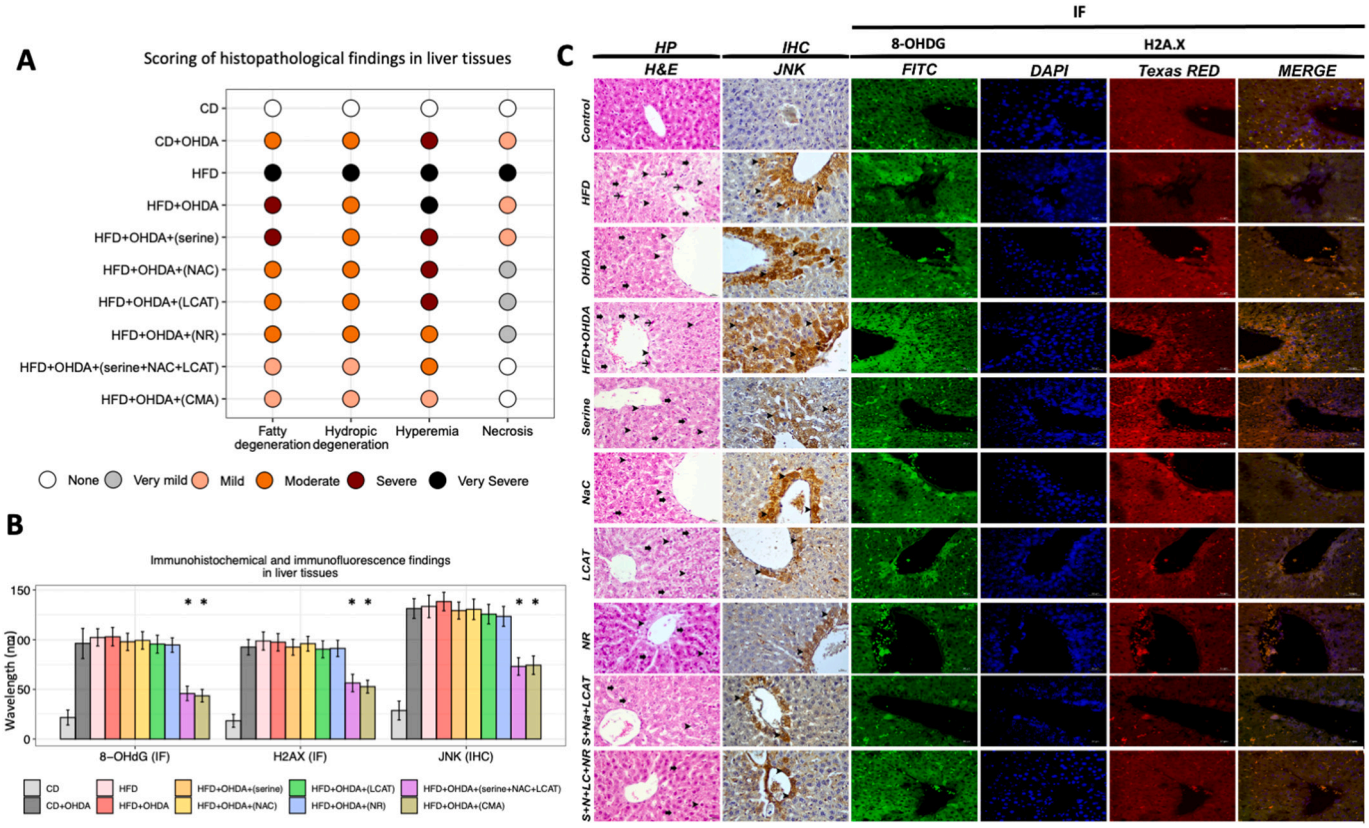

Fig. 7. Immunohistopathological examination of liver tissues in PD-like animal model.
A) Plot shows histopathological findings in liver (acinar regions) tissues. **B)** Bar plot shows immunohistochemical and immunofluorescent findings in liver tissue. **C)** Histopathological (Haematoxylin &Eosin), immunohistochemical (JNK) and immunofluorescence (FITC, DAPI, Texas Red and merged) images of rat liver tissue (antibodies: 8OHDG and H2A.X). Slides evaluated by two independent pathologists. Histopathological scores were: None (−), very mild (+), mild (++), moderate (+++), severe (++++) and very severe (+++++). In order to determine the intensity of positive staining from the obtained images, 5 random areas were selected from each image. For immunohistochemical and immunofluorescent images, the positive/total area was calculated by measuring with the ZEISS Zen Imaging Software program. Data were statistically defined as mean and standard deviation (mean ± SD) for % area. CD: chow diet, 6-OHDA: 6-hydroxydopamine hydrochloride, HFD: high-fat diet, NAC: *N*-acetyl-L-cysteine, LCAT: L-carnitine tartrate, NR: nicotinamide riboside, IF: Immunofluorescence, IHC: Immunohistochemistry. (For interpretation of the references to colour in this figure legend, the reader is referred to the web version of this article.)

improvements in neurological and metabolic functions with individual metabolic activators both in the brain and liver tissues of animals, but the effect was superior with the administration of CMA both in brain and liver tissues.

4. Discussion

Despite the wide range of clinical presentations, NDDs have several characteristics in common, such as progression of symptoms and molecular mechanisms of pathophysiology. Specific brain subregions are impaired in neurodegenerative disorders, which emerge slowly but steadily [53]. Due to the difficulties in setting out an experimental procedure that captures the intricacies of the human nervous system, animal modelling is the main prerequisite for gaining relevant insights and developing hypotheses [54]. Here, we first analysed brain transcriptomics data from AD patients and controls in the ROSMAP cohort and found that mitochondrial dysfunction is one of the underlying molecular mechanisms of AD, consistent with previous metabolomics studies in humans [55,56] and rats [57]. Consequently, we examined the effect of CMA administration in AD- and PD-like animal models and showed that CMA improved metabolic parameters and behavioural scores in parallel to the neurohistological outcomes. A graphical presentation of study designs with key findings is shown in Fig. S1.

Metabolic dysregulation is a significant risk factor for NDDs. Disturbance in glucose homeostasis, lipid metabolism, mitochondrial dysfunction and endoplasmic reticulum stress are linked to mental deterioration parallel to neuronal dysfunctions in AD and PD [58,59]. Numerous investigations have been performed to reveal the effect of diabetes on the brain by using animals with decreased insulin production and persistent hyperglycaemia [60–63]. The most widely studied model is developed by the infusion of STZ, which leads to beta cell death and causes neurotoxicity, triggering memory deficits associated with impaired synaptic plasticity and altered brain metabolism [64,65].

Animal models that mimic specific diseases, such as AD and PD, are essential for studying the disease mechanisms and developing potential treatments. In our research, we used female Sprague Dawley rats to create an AD-like rat model and female Wistar rats to create a PD-like rat model. Previous studies have shown that Sprague Dawley rats are more susceptible to chemically-induced memory and learning impairments. On the other hand, Wistar rats have been found to have higher motor activity performance than Sprague Dawley rats at all ages tested [66]. In the existing scientific literature, there are several different animal models used to study AD, many of which are based on genetic mutations that have been observed in familial AD. However, the most common form of AD is the sporadic, or late-onset form of the disease. This type of AD is influenced by a combination of genetic, environmental, and lifestyle factors. In the early 1990s, researchers discovered that impaired insulin signaling and glucose metabolism in the brain could lead to cognitive dysfunction. Since then, intracerebroventricular injection of STZ has been widely used in animal models to demonstrate impaired neuronal plasticity and learning deficits caused by metabolic diseases [67–69]. Moreover, rodent models fed with high-fat diets exhibited all

the hallmarks of these degenerative diseases and represented an interesting approach to the study of the phenotypic features and pathogenic mechanisms of NDDs [70,71]. Recently, several genetic models have been suggested with their advantages including capturing both Aβ and phospho-tau as well as maintaining aging features of AD, but high lethality, overexpression of tau protein and limited cognitive impairment were seen in genetic models [72]. In the case of PD, 6-OHDA has been commonly used in animal models because of it produces consistent behavioural changes and predictable degeneration in dopaminergic neurons [73]. While these neurotoxic models are effective at studying the degeneration of the nigrostriatal pathway, there are some notable differences between the model and human PD, such as the rapid progression of dopaminergic neuron degeneration and the absence of Lewy bodies [74]. Transgenic models, on the other hand, can provide insight into the causes of PD, but they have limitations, such as the lack of consistent neuronal loss in the substantia nigra and variable phenotypes among lines with the same mutations [75]. Moreover, the difficulty and cost of the maintenance of transgenic rat colonies has limited their wider use both in AD and PD research.

The liver is the major regulator organ which controls body energy homeostasis by neuronal and hormonal signals. In this context, liver pathologies promote neurological diseases due to the established connectivity between the hepatic and the central nervous system, known as the brain-liver axis [76–78]. There have been several publications reporting patients or animal models with hepatic disorders shows cerebral deficits and neurological dysfunction analogous to NDD features [4,23]. Moreover, it has been shown that HFD generated neuropathological characteristics similar to AD in normal mice, and promoted plaque development in an AD mouse model [23,79]. Considering the association between the liver pathologies and declined cognition in NDD patients, recovering from deleterious effects of metabolic disorders is a promising treatment strategy for neurodegenerative diseases. In our previous studies, we reported that CMA administration effectively promotes mitochondrial fatty acid uptake from the cytosol, facilitates fatty acid oxidation in the mitochondria, and alleviates oxidative stress by de novo glutathione generation in metabolic diseases [27,29–33]. The present work highlights the effect of CMA administration in the animal models of AD and PD and observed that CMA administration significantly improved the metabolic and histological parameters associated with the NDDs both in brain and liver tissues.

Literature also shows that vascular dysfunction has also been implicated in the pathophysiology of NDDs and dementia [80]. Vascular abnormalities such as microvascular failures, neurovascular deficits, and impaired BBB integrity are also associated with NDDs [81,82]. Microvascular dysfunction reduces cerebral blood flow, the brain's oxygen supply and the availability of energy molecules and nutrients. Based on our findings, CMA supplementation substantially influences hyperemia, degeneration, and necrosis in the neurons. In parallel to the improvement in brain metabolism, we also observed dramatic improvement in liver metabolism after CMA administration.

Oxidative stress is caused by an imbalance in the antioxidant defence system and the intracellular formation of reactive oxygen species, leading to memory impairments. While decreased synaptic reorganization in neural networks leads to cognitive problems in old age, whether such a mechanism is regulated by oxidative stress and which pathways are implicated are yet unknown. Preserving redox homeostasis in elderly animals might protect the biological processes underpinning cognitive decline, particularly by preserving NMDA-R activation via the D-serine-dependent route [5]. Long-term NAC administration has been shown to restore D-serine-dependent NMDA-R activation and reduce oxidative injury in the hippocampal region of aged rats [5]. Similarly, NAC therapy showed a neuroprotective impact on dopaminergic degeneration and neuroinflammatory response in the nigrostriatal pathway in the animal model [83]. Neuroprotective techniques are becoming more critical in slowing dopaminergic cell damage and inflammatory responses associated with increasing neurodegeneration in NDDs. Our findings pave the way for more prominent research to establish its prospective efficacy as a neuroprotective technique.

NAD^+ is a critical metabolite that plays a role in cellular energy homeostasis, adaptation to stress stimuli and cell viability [84]. Synaptic plasticity and neural stress tolerance are mediated by several NAD^+-dependent enzymes. In animal models of AD and PD, NAD^+ precursors like NR and NMN improve memory and learning while increasing longevity [85]. Recent studies provide evidence that enhancing NAD^+ levels can restore the impaired brain-energy metabolism and oxidative stress that are implicated in cognitive decline. For instance: 1) Activation of HCAR2 with niacin in 5xFAD mice reduced plaque burden and neuronal dystrophy, attenuated neuronal loss and improved working memory deficits [6]; 2) NAD^+ supplementation with NR significantly normalized neuroinflammation, synaptic transmission, phosphorylated Tau and DNA damage as well as rescued the learning and motor functions in a 3xTgAD/Polβ+/− AD mouse model [7]; 3) High levels of ectopic cytoplasmic DNA in APP/PS1 mutant mice and human AD fibroblasts were down-regulated with NR treatment, which induced mitophagy and improved cognitive and synaptic functions in APP/PS1 mutant mice [8]. Similarly, mitochondrial damage is a key feature that is boosted by NR in neurons derived from PD patients' stem cells [9]. Furthermore, NR is found to be neuroprotective in fly models of PD [9]. Moreover, a human phase I trial of NAD replenishment therapy with oral NR in PD showed increased cerebral NAD levels, and this was associated with improved brain metabolism and clinical improvement [11]. Overall, the findings nominate NR as a potential neuroprotective treatment for NDDs.

Metabolic imbalance in brain aerobic glycolysis is frequently seen in the early stages of AD [86]. However, how this contributes to both structural and cognitive abnormalities is unknown. Growing evidence suggests that L-serine regulates the release of several cytokines in the brain to repair cognitive function, regulate cerebral blood flow, alleviate inflammation, enhance remyelination, and facilitate other neuroprotective effects on neurological impairments [87]. A recent study reveals that astrocytic glycolysis controls cognitive functions through synaptic NMDA receptors and suggests oral L-serine as an accessible therapy for AD [10]. Recently, a conflicting study about the increased de novo serine synthesis in AD patients has been published [88]. However, the authors did not measure the plasma and cerebrospinal fluid level of the serine and did not proved additional validation [89]. Based on our analysis, we found that supplementation of serine only significantly improved metabolic functions and as well histopathological parameters in the AD- and PD-like animal models.

Lipids play crucial roles in cell signaling and various physiological processes, especially in the brain. Impaired lipid metabolism in the brain has been implicated in NDDs [90]. In a recent study, plasma lipidome is found to be dysregulated in AD and it is associated with disease genetic risk factors [91]. We found significant reductions in plasma TG, cholesterol and LDL levels in the CMA-treated animals.

One possible limitation of the study is the small sample size per group that a larger sample size would be better for statistical analysis. However, this is a comprehensive study with 20 groups with behavioural and pathological evaluations (simultaneous exposure, oral gavage, sacrificing, tissue sampling etc. in time). Another limitation is that we couldn't evaluate the insulin levels due to the technical limitations on providing appropriate kits for rats in our country during the study time.

Here, we reported that improving mitochondrial metabolism with formulation of CMA, reduced hyperemia, degeneration and necrosis in neurons and improved behavioural functions in the rat models. Thus, we propose that CMA is a promising therapeutic agent for NDDs with a high translational potential for clinical trials. In addition, we believe that this work sets the stage for further work, using targets to improve NAD+ and glutathione metabolism for treating NDDs. These will lead more therapeutic strategies to modulate mitochondrial functions in NDDs through the promotion of mitochondrial fatty acid oxidation and related

pathways, which is required for an efficient mitochondrial response to neurodegenerative pathology.

In conclusion, in relevant metabolic models of AD and PD, we have demonstrated that CMA administration improved behavioural outcomes in parallel with the neurohistological outcome in the brain and liver. The most significant beneficial effects on histopathological and clinical outcomes observed after the CMA treatment showed the importance of targeting multiple metabolic pathways in the neuroprotective treatment of NDDs.

Supplementary data to this article can be found online at https://doi.org/10.1016/j.lfs.2022.121325.

Funding

This work was financially supported by ScandiBio Therapeutics and Knut and Alice Wallenberg Foundation.

Declaration of competing interest

AM, JB and MU are the founder and shareholders of ScandiBio Therapeutics. The other authors declare no competing interests.

Data availability

All code used for the analyses and transcriptomics analysis results are available in https://github.com/sysmedicine/NDDanimal (accessed on 26 Sep 2022).

Acknowledgments

This work was financially supported by ScandiBio Therapeutics and Knut and Alice Wallenberg Foundation. The authors would like to thank ChromaDex Inc. (Irvine, CA, USA) for providing NR. AM and HY acknowledge support from the PoLiMeR Innovative Training Network (Marie Sklodowska-Curie Grant Agreement No. 812616), which has received funding from the European Union's Horizon 2020 research and innovation programme. The computations were performed on resources provided by SNIC through Uppsala Multidisciplinary Center for Advanced Computational Science (UPPMAX) under Project sllstore2017024.

References

[1] Organisation WH, Dementia, Available from, https://www.who.int/news-room/fact-sheets/detail/dementia, 2022.
[2] S. Azam, M.E. Haque, R. Balakrishnan, I.-S. Kim, D.-K. Choi, The ageing brain: molecular and cellular basis of neurodegeneration, Front.Cell Dev.Biol. 9 (2021) 683459.
[3] D.A. Butterfield, B. Halliwell, Oxidative stress, dysfunctional glucose metabolism and Alzheimer disease, Nat. Rev. Neurosci. 20 (3) (2019) 148–160.
[4] M.F. Bassendine, S.D. Taylor-Robinson, M. Fertleman, M. Khan, D. Neely, Is Alzheimer's disease a liver disease of the brain? J. Alzheimers Dis. 75 (1) (2020) 1–14.
[5] C. Haxaire, F.R. Turpin, B. Potier, M. Kervern, P.M. Sinet, G. Barbanel, et al., Reversal of age-related oxidative stress prevents hippocampal synaptic plasticity deficits by protecting D-serine-dependent NMDA receptor activation, Aging Cell 11 (2) (2012) 336–344.
[6] M. Moutinho, S.S. Puntambekar, A.P. Tsai, I. Coronel, P.B. Lin, B.T. Casali, et al., The niacin receptor HCAR2 modulates microglial response and limits disease progression in a mouse model of Alzheimer's disease, Sci. Transl. Med. 14 (637) (2022), eabl7634.
[7] Y. Hou, S. Lautrup, S. Cordonnier, Y. Wang, D.L. Croteau, E. Zavala, et al., NAD(+) supplementation normalizes key Alzheimer's features and DNA damage responses in a new AD mouse model with introduced DNA repair deficiency, Proc. Natl. Acad. Sci. U. S. A. 115 (8) (2018) E1876–E1885.
[8] Y. Hou, Y. Wei, S. Lautrup, B. Yang, Y. Wang, S. Cordonnier, et al., NAD(+) supplementation reduces neuroinflammation and cell senescence in a transgenic mouse model of Alzheimer's disease via cGAS-STING, Proc. Natl. Acad. Sci. U. S. A. 118 (37) (2021), e2011226118.
[9] D.C. Schöndorf, D. Ivanyuk, P. Baden, A. Sanchez-Martinez, S. De Cicco, C. Yu, et al., The NAD+ precursor nicotinamide riboside rescues mitochondrial defects and neuronal loss in iPSC and fly models of Parkinson's disease, Cell Rep. 23 (10) (2018) 2976–2988.
[10] J. Le Douce, M. Maugard, J. Veran, M. Matos, P. Jégo, P.A. Vigneron, et al., Impairment of glycolysis-derived l-serine production in astrocytes contributes to cognitive deficits in Alzheimer's disease, Cell Metab. 31 (3) (2020) 503–517.e8.
[11] B. Brakedal, C. Dölle, F. Riemer, Y. Ma, G.S. Nido, G.O. Skeie, et al., The NADPARK study: a randomized phase I trial of nicotinamide riboside supplementation in Parkinson's disease, Cell Metab. 34 (3) (2022) 396–407.e6.
[12] W.M. Caudle, T.K. Bammler, Y. Lin, S. Pan, J. Zhang, Using 'omics' to define pathogenesis and biomarkers of Parkinson's disease, Expert. Rev. Neurother. 10 (6) (2010) 925–942.
[13] R.M. Miller, G.L. Kiser, T.M. Kaysser-Kranich, R.J. Lockner, C. Palaniappan, H. J. Federoff, Robust dysregulation of gene expression in substantia nigra and striatum in Parkinson's disease, Neurobiol. Dis. 21 (2) (2006) 305–313.
[14] D.C. Duke, L.B. Moran, M.E. Kalaitzakis, M. Deprez, D.T. Dexter, R.K. Pearce, et al., Transcriptome analysis reveals link between proteasomal and mitochondrial pathways in Parkinson's disease, Neurogenetics 7 (3) (2006) 139–148.
[15] N. Ruffini, S. Klingenberg, S. Schweiger, S. Gerber, Common factors in neurodegeneration: a meta-study revealing shared patterns on a multi-omics scale, Cells 9 (12) (2020).
[16] I. Aracil-Bolaños, F. Sampedro, J. Marín-Lahoz, A. Horta-Barba, S. Martínez-Horta, M. Botí, et al., A divergent breakdown of neurocognitive networks in Parkinson's disease mild cognitive impairment, Hum. Brain Mapp. 40 (11) (2019) 3233–3242.
[17] I. Aracil-Bolaños, F. Sampedro, J. Pujol, C. Soriano-Mas, J.M. Gónzalez-de-Echávarri, J. Kulisevsky, et al., The impact of dopaminergic treatment over cognitive networks in Parkinson's disease: stemming the tide? Hum. Brain Mapp. 42 (17) (2021) 5736–5746.
[18] L. Christopher, S. Duff-Canning, Y. Koshimori, B. Segura, I. Boileau, R. Chen, et al., Salience network and parahippocampal dopamine dysfunction in memory-impaired Parkinson disease, Ann. Neurol. 77 (2) (2015) 269–280.
[19] U. Saxena, Bioenergetics failure in neurodegenerative diseases: back to the future, Expert Opin. Ther. Targets 16 (4) (2012) 351–354.
[20] R. Chianese, R. Coccurello, A. Viggiano, M. Scafuro, M. Fiore, G. Coppola, et al., Impact of dietary fats on brain functions, Curr. Neuropharmacol. 16 (7) (2018) 1059–1085.
[21] C.I.F. Janssen, D. Jansen, M.P.C. Mutsaers, P.J.W.C. Dederen, B. Geenen, M. T. Mulder, et al., The effect of a high-fat diet on brain plasticity, inflammation and cognition in female ApoE4-knockin and ApoE-knockout mice, PloS one 11 (5) (2016), e0155307-e.
[22] N. Del Olmo, M. Ruiz-Gayo, Influence of high-fat diets consumed during the juvenile period on hippocampal morphology and function, Front. Cell. Neurosci. 12 (2018).
[23] C.R. Bosoi, M. Vandal, M. Tournissac, M. Leclerc, H. Fanet, P.L. Mitchell, et al., High-fat diet modulates hepatic amyloid β and cerebrosterol metabolism in the triple transgenic mouse model of Alzheimer's disease, Hepatol. Commun. 5 (3) (2021) 446–460.
[24] G.C. de Paula, H.S. Brunetta, D.F. Engel, J.M. Gaspar, L.A. Velloso, D. Engblom, et al., Hippocampal function is impaired by a short-term high-fat diet in mice: increased blood-brain barrier permeability and neuroinflammation as triggering events, Front. Neurosci. 15 (2021), 734158.
[25] J. Han, P. Nepal, A. Odelade, F.D. Freely, D.M. Belton, J.L. Graves Jr., et al., High-fat diet-induced weight gain, behavioral deficits, and dopamine changes in young C57BL/6J mice, Front Nutr. 7 (2021), 591161.
[26] N.R.W. Cleland, S.I. Al-Juboori, E. Dobrinskikh, K.D. Bruce, Altered substrate metabolism in neurodegenerative disease: new insights from metabolic imaging, J. Neuroinflammation 18 (1) (2021) 248.
[27] A. Mardinoglu, R. Agren, C. Kampf, A. Asplund, M. Uhlen, J. Nielsen, Genome-scale metabolic modelling of hepatocytes reveals serine deficiency in patients with non-alcoholic fatty liver disease, Nat. Commun. 5 (2014) 3083.
[28] A. Mardinoglu, E. Bjornson, C. Zhang, M. Klevstig, S. Söderlund, M. Ståhlman, et al., Personal model-assisted identification of NAD(+) and glutathione metabolism as intervention target in NAFLD, Mol. Syst. Biol. 13 (3) (2017) 916.
[29] C. Zhang, E. Bjornson, M. Arif, A. Tebani, A. Lovric, R. Benfeitas, et al., The acute effect of metabolic cofactor supplementation: a potential therapeutic strategy against non-alcoholic fatty liver disease, Mol. Syst. Biol. 16 (4) (2020), e9495.
[30] A. Mardinoglu, D. Ural, M. Zeybel, H.H. Yuksel, M. Uhlén, J. Borén, The potential use of metabolic cofactors in treatment of NAFLD, Nutrients 11 (7) (2019) 1578.
[31] A. Mardinoglu, J. Boren, U. Smith, M. Uhlen, J. Nielsen, Systems biology in hepatology: approaches and applications, Nat. Rev. Gastroenterol. Hepatol. 15 (6) (2018) 365–377.
[32] O. Altay, M. Arif, X. Li, H. Yang, M. Aydın, G. Alkurt, et al., Combined metabolic activators accelerates recovery in mild-to-moderate COVID-19, Adv. Sci. n/a (n/a) (2021), 2101222.
[33] A. Mardinoglu, H. Wu, E. Bjornson, C. Zhang, A. Hakkarainen, S.M. Rasanen, et al., An integrated understanding of the rapid metabolic benefits of a carbohydrate-restricted diet on hepatic steatosis in humans, Cell Metab. 27 (3) (2018) 559–71 e5.
[34] H. Yang, J. Mayneris-Perxachs, N. Boqué, J.M. Del Bas, L. Arola, M. Yuan, et al., Combined metabolic activators decrease liver steatosis by activating mitochondrial metabolism in hamsters fed with a high-fat diet, Biomedicines 9 (10) (2021).
[35] A.J. Myers, J.R. Gibbs, J.A. Webster, K. Rohrer, A. Zhao, L. Marlowe, et al., A survey of genetic human cortical gene expression, Nat. Genet. 39 (12) (2007) 1494–1499.
[36] J.A. Webster, J.R. Gibbs, J. Clarke, M. Ray, W. Zhang, P. Holmans, et al., Genetic control of human brain transcript expression in Alzheimer disease, Am. J. Hum. Genet. 84 (4) (2009) 445–458.
[37] S. Mostafavi, C. Gaiteri, S.E. Sullivan, C.C. White, S. Tasaki, J. Xu, et al., A molecular network of the aging human brain provides insights into the pathology

and cognitive decline of Alzheimer's disease, Nat. Neurosci. 21 (6) (2018) 811–819.
[38] M.E. Ritchie, B. Phipson, D. Wu, Y. Hu, C.W. Law, W. Shi, et al., Limma powers differential expression analyses for RNA-sequencing and microarray studies, Nucleic Acids Res. 43 (7) (2015), e47.
[39] M.I. Love, W. Huber, S. Anders, Moderated estimation of fold change and dispersion for RNA-seq data with DESeq2, Genome Biol. 15 (12) (2014) 550.
[40] K.L. Howe, P. Achuthan, J. Allen, J. Allen, J. Alvarez-Jarreta, M.R. Amode, et al., Ensembl 2021, Nucleic Acids Res. 49 (D1) (2020) D884–D891.
[41] L. Väremo, J. Nielsen, I. Nookaew, Enriching the gene set analysis of genome-wide data by incorporating directionality of gene expression and combining statistical hypotheses and methods, Nucleic Acids Res. 41 (8) (2013) 4378–4391.
[42] R. Agren, L. Liu, S. Shoaie, W. Vongsangnak, I. Nookaew, J. Nielsen, The RAVEN toolbox and its use for generating a genome-scale metabolic model for Penicillium chrysogenum, PLoS Comput. Biol. 9 (3) (2013), e1002980.
[43] S. Lam, N. Hartmann, R. Benfeitas, C. Zhang, M. Arif, H. Turkez, et al., Systems Analysis Reveals Ageing-related Perturbations in Retinoids and Sex Hormones in Alzheimer's and Parkinson's Diseases, bioRxiv, 2021, 2021.06.10.447367.
[44] M. Kanehisa, Y. Sato, KEGG Mapper for inferring cellular functions from protein sequences, Protein Sci. 29 (1) (2020) 28–35.
[45] L.J. Pellegrino, A.J. Cushman, A.S. Pellegrino, A Stereotaxic Atlas of the Rat Brain, 2nd ed., Plenum Press, New York (N.Y.), 1979, 1967 ed.
[46] R. Vajdi-Hokmabad, M. Ziaee, S. Sadigh-Eteghad, S. Sandoghchian Shotorbani, J. Mahmoudi, Modafinil improves catalepsy in a rat 6-hydroxydopamine model of Parkinson's disease; possible involvement of dopaminergic neurotransmission, Adv. Pharm. Bull. 7 (3) (2017) 359–365.
[47] H. Boracı, Ö. Kirazlı, R. Gülhan, D. Yıldız Sercan, Ü.S. Şehirli, Neuroprotective effect of regular swimming exercise on calretinin-positive striatal neurons of Parkinsonian rats, Anat. Sci. Int. 95 (4) (2020) 429–439.
[48] G. Paxinos, C. Watson, The Rat Brain in Stereotaxic Coordinates, hard cover edition, Elsevier, 2006.
[49] K. Miyanishi, M.E. Choudhury, M. Watanabe, M. Kubo, M. Nomoto, H. Yano, et al., Behavioral tests predicting striatal dopamine level in a rat hemi-Parkinson's disease model, Neurochem. Int. 122 (2019) 38–46.
[50] I. Creese, R. Burt David, Solomon H. Snyder, Dopamine receptor binding enhancement accompanies lesion-induced behavioral supersensitivity, Science 197 (4303) (1977) 596–598.
[51] R. Iancu, P. Mohapel, P. Brundin, G. Paul, Behavioral characterization of a unilateral 6-OHDA-lesion model of Parkinson's disease in mice, Behav. Brain Res. 162 (1) (2005) 1–10.
[52] A. Mardinoglu, R. Agren, C. Kampf, A. Asplund, I. Nookaew, P. Jacobson, et al., Integration of clinical data with a genome-scale metabolic model of the human adipocyte, Mol. Syst. Biol. 9 (2013) 649.
[53] T. Guo, D. Zhang, Y. Zeng, T.Y. Huang, H. Xu, Y. Zhao, Molecular and cellular mechanisms underlying the pathogenesis of Alzheimer's disease, Mol. Neurodegener. 15 (1) (2020) 40.
[54] T.M. Dawson, T.E. Golde, C. Lagier-Tourenne, Animal models of neurodegenerative diseases, Nat. Neurosci. 21 (10) (2018) 1370–1379.
[55] B. Bai, X. Wang, Y. Li, P.C. Chen, K. Yu, K.K. Dey, et al., Deep multilayer brain proteomics identifies molecular networks in Alzheimer's disease progression, Neuron 105 (6) (2020) 975–991.e7.
[56] Z. Huo, L. Yu, J. Yang, Y. Zhu, D.A. Bennett, J. Zhao, Brain and blood metabolome for Alzheimer's dementia: findings from a targeted metabolomics analysis, Neurobiol. Aging 86 (2020) 123–133.
[57] M. Wei, Y. Liu, Z. Pi, K. Yue, S. Li, M. Hu, et al., Investigation of plasma metabolomics and neurotransmitter dysfunction in the process of Alzheimer's disease rat induced by amyloid beta 25–35, RSC Adv. 9 (32) (2019) 18308–18319.
[58] M. Spinelli, S. Fusco, C. Grassi, Brain insulin resistance and hippocampal plasticity: mechanisms and biomarkers of cognitive decline, Front. Neurosci. 13 (2019) 788.
[59] S.K. Jha, N.K. Jha, D. Kumar, R.K. Ambasta, P. Kumar, Linking mitochondrial dysfunction, metabolic syndrome and stress signaling in Neurodegeneration, Biochim. Biophys. Acta (BBA) - Mol. Basis Dis. 1863 (5) (2017) 1132–1146.
[60] S. Rom, V. Zuluaga-Ramirez, S. Gajghate, A. Seliga, M. Winfield, N.A. Heldt, et al., Hyperglycemia-driven neuroinflammation compromises BBB leading to memory loss in both diabetes mellitus (DM) type 1 and type 2 mouse models, Mol. Neurobiol. 56 (3) (2019) 1883–1896.
[61] R.A. Wirt, L.A. Crew, A.A. Ortiz, A.M. McNeela, E. Flores, J.W. Kinney, et al., Altered theta rhythm and hippocampal-cortical interactions underlie working memory deficits in a hyperglycemia risk factor model of Alzheimer's disease, Commun.Biol.. 4 (1) (2021) 1036.
[62] E. Ferreiro, M. Lanzillo, D. Canhoto, A.M. Carvalho da Silva, S.I. Mota, I.S. Dias, et al., Chronic hyperglycemia impairs hippocampal neurogenesis and memory in an Alzheimer's disease mouse model, Neurobiol. Aging 92 (2020) 98–113.
[63] A.A. Ortiz, A. Platt, J.W. Kinney, Examining the effects of a blood glucose rescue on Alzheimer's disease-related pathology in hyperglycemic mice, Alzheimers Dement. 17 (S3) (2021), e057639.
[64] A. Kamal, G.J. Biessels, I.J. Urban, W.H. Gispen, Hippocampal synaptic plasticity in streptozotocin-diabetic rats: impairment of long-term potentiation and facilitation of long-term depression, Neuroscience 90 (3) (1999) 737–745.
[65] C.C. Qi, X.X. Chen, X.R. Gao, J.X. Xu, S. Liu, J.F. Ge, Impaired learning and memory ability induced by a bilaterally hippocampal injection of streptozotocin in mice: involved with the adaptive changes of synaptic plasticity, Front. Aging Neurosci. 13 (2021), 633495.
[66] A. Zmarowski, M. Beekhuijzen, J. Lensen, H. Emmen, Differential performance of Wistar Han and Sprague Dawley rats in behavioral tests: differences in baseline behavior and reactivity to positive control agents, Reprod. Toxicol. 34 (2) (2012) 192–203.
[67] Y. Zhang, R. Ding, S. Wang, Z. Ren, L. Xu, X. Zhang, et al., Effect of intraperitoneal or intracerebroventricular injection of streptozotocin on learning and memory in mice, Exp. Ther. Med. 16 (3) (2018) 2375–2380.
[68] Y. Chen, Z. Liang, Z. Tian, J. Blanchard, C.L. Dai, S. Chalbot, et al., Intracerebroventricular streptozotocin exacerbates Alzheimer-like changes of 3xTg-AD mice, Mol. Neurobiol. 49 (1) (2014) 547–562.
[69] M. Fan, S. Liu, H.-M. Sun, M.-D. Ma, Y.-J. Gao, C.-C. Qi, et al., Bilateral intracerebroventricular injection of streptozotocin induces AD-like behavioral impairments and neuropathological features in mice: involved with the fundamental role of neuroinflammation, Biomed. Pharmacother. 153 (2022), 113375.
[70] C.P.E. Rollins, D. Gallino, V. Kong, G. Ayranci, G.A. Devenyi, J. Germann, et al., Contributions of a high-fat diet to Alzheimer's disease-related decline: a longitudinal behavioural and structural neuroimaging study in mouse models, Neuroimage Clin. 21 (2019), 101606.
[71] A. Amelianchik, L. Sweetland-Martin, E.H. Norris, The effect of dietary fat consumption on Alzheimer's disease pathogenesis in mouse models, Transl. Psychiatry 12 (1) (2022) 293.
[72] A.M. Foley, Z.M. Ammar, R.H. Lee, C.S. Mitchell, Systematic review of the relationship between amyloid-β levels and measures of transgenic mouse cognitive deficit in Alzheimer's disease, J. Alzheimers Dis. 44 (3) (2015) 787–795.
[73] S.J. Chia, E.K. Tan, Y.X. Chao, Historical perspective: models of Parkinson's disease, Int. J. Mol. Sci. 21 (7) (2020).
[74] K. Tieu, A guide to neurotoxic animal models of Parkinson's disease, Cold Spring Harb. Perspect. Med. 1 (1) (2011), a009316.
[75] J. Blesa, S. Przedborski, Parkinson's disease: animal models and dopaminergic cell vulnerability, Front. Neuroanat. 8 (2014) 155.
[76] R. Bordet, D. Deplanque, Brain–liver axis: a new pathway for cognitive disorders related to hepatic fibrosis, Eur. J. Neurol. 27 (11) (2020) 2111–2112.
[77] R.F. Butterworth, The liver-brain axis in liver failure: neuroinflammation and encephalopathy, Nat. Rev. Gastroenterol. Hepatol. 10 (9) (2013) 522–528.
[78] P.I. Mighiu, B.M. Filippi, T.K.T. Lam, Linking inflammation to the brain-liver axis, Diabetes 61 (6) (2012) 1350–1352.
[79] D.G. Kim, A. Krenz, L.E. Toussaint, K.J. Maurer, S.A. Robinson, A. Yan, et al., Non-alcoholic fatty liver disease induces signs of Alzheimer's disease (AD) in wild-type mice and accelerates pathological signs of AD in an AD model, J. Neuroinflammation 13 (2016) 1.
[80] J. Klohs, An integrated view on vascular dysfunction in Alzheimer's disease, Neurodegener. Dis. 19 (3–4) (2019) 109–127.
[81] A.R. Nelson, M.D. Sweeney, A.P. Sagare, B.V. Zlokovic, Neurovascular dysfunction and neurodegeneration in dementia and Alzheimer's disease, Biochim. Biophys. Acta 1862 (5) (2016) 887–900.
[82] M.T. Uemura, T. Maki, M. Ihara, V.M.Y. Lee, J.Q. Trojanowski, Brain microvascular pericytes in vascular cognitive impairment and dementia, Front. Aging Neurosci. (2020) 12.
[83] A.-L. Gil-Martínez, L. Cuenca, C. Sánchez, C. Estrada, E. Fernández-Villalba, M. T. Herrero, Effect of NAC treatment and physical activity on neuroinflammation in subchronic parkinsonism; is physical activity essential? J. Neuroinflammation 15 (1) (2018) 328.
[84] N. Xie, L. Zhang, W. Gao, C. Huang, P.E. Huber, X. Zhou, et al., NAD(+) metabolism: pathophysiologic mechanisms and therapeutic potential, Signal Transduct. Target. Ther. 5 (1) (2020) 227.
[85] E.F. Fang, S. Lautrup, Y. Hou, T.G. Demarest, D.L. Croteau, M.P. Mattson, et al., NAD(+) in aging: molecular mechanisms and translational implications, Trends Mol. Med. 23 (10) (2017) 899–916.
[86] A.G. Vlassenko, M.E. Raichle, Brain aerobic glycolysis functions and Alzheimer's disease, Clin. Transl. Imaging 3 (1) (2015) 27–37.
[87] L. Ye, Y. Sun, Z. Jiang, G. Wang, L-serine, an endogenous amino acid, is a potential neuroprotective agent for neurological disease and injury, Front. Mol. Neurosci. 14 (2021), 726665.
[88] X. Chen, R. Calandrelli, J. Girardini, Z. Yan, Z. Tan, X. Xu, et al., PHGDH expression increases with progression of Alzheimer's disease pathology and symptoms, Cell Metab. 34 (5) (2022) 651–653.
[89] G. Bonvento, S.H.R. Oliet, A. Panatier, Glycolysis-derived L-serine levels versus PHGDH expression in Alzheimer's disease, Cell Metab. 34 (5) (2022) 654–655.
[90] Q. Liu, J. Zhang, Lipid metabolism in Alzheimer's disease, Neurosci. Bull. 30 (2) (2014) 331–345.
[91] Y. Liu, A. Thalamuthu, K.A. Mather, J. Crawford, M. Ulanova, M.W.K. Wong, et al., Plasma lipidome is dysregulated in Alzheimer's disease and is associated with disease risk genes, Transl. Psychiatry 11 (1) (2021) 344.